

Probabilistic computation with emerging covariance: towards efficient uncertainty quantification

Hengyuan Ma¹, Yang Qi^{1,2,3}, Li Zhang⁴, Wenlian Lu^{1,2}, Jianfeng Feng^{1,2,*}

1 Institute of Science and Technology for Brain-inspired Intelligence, Fudan University, Shanghai 200433, China

2 Key Laboratory of Computational Neuroscience and Brain-Inspired Intelligence (Fudan University), Ministry of Education, China

3 MOE Frontiers Center for Brain Science, Fudan University, Shanghai 200433, China

4 School of Data Science, Fudan University, Shanghai 200433, China

** jffeng@fudan.edu.cn*

ABSTRACT

Building robust, interpretable, and secure artificial intelligence system requires some degree of quantifying and representing uncertainty via a probabilistic perspective, as it allows to mimic human cognitive abilities. However, probabilistic computation presents significant challenges due to its inherent complexity. In this paper, we develop an efficient and interpretable probabilistic computation framework by truncating the probabilistic representation up to its first two moments, i.e., mean and covariance. We instantiate the framework by training a deterministic surrogate of a stochastic network that learns the complex probabilistic representation via combinations of simple activations, encapsulating the non-linearities coupling of the mean and covariance. We show that when the mean is supervised for optimizing the task objective, the unsupervised covariance spontaneously emerging from the non-linear coupling with the mean faithfully captures the uncertainty associated with model predictions. Our research highlights the inherent computability and simplicity of probabilistic computation, enabling its wider application in large-scale settings.

Uncertainty is an inherent and omnipresent aspect of decision-making, arising from various sources such as the environment, observed data, learning process, and the model itself. While humans are capable of incorporating such uncertainty into their decision-making by considering a confidence level, it is not an easy task for current artificial neural networks (ANNs) to evaluate the level of uncertainty associated with their predictions. This challenge arises from one of the fundamental distinctions between information processing in the human brain and in ANNs: unlike the deterministic approach followed by von Neumann computers, which are commonly used to implement ANNs, the brain employs random mechanisms to process information [1]. Emulating the brain's approach to information processing is one of the most viable ways to achieve artificial general intelligence (AGI)-type computation [2]. *Probabilistic computation* is a class of learning algorithms that leverage probability theory and statistics to represent and manipulate uncertainty [3]. In contrast to the deterministic computation, probabilistic computation offers the ability to not only produce inference but also to quantify the uncertainty associated with that inference. This capability is essential for constructing more robust, trustworthy, and interpretable ANNs that can mimic human reasoning and decision-making [4, 5].

Exact probabilistic computations involving functional operators on probability density functions are incomputable. To overcome this challenge, Bayesian variational inference (BVI) [6] is introduced as an approximation method. BVI employs a parameterized variational distribution and minimizes a variational loss. However, evaluating the gradient of the variational loss for optimization can be difficult. This problem is alleviated by Monte Carlo (MC) methods [7, 8, 9, 10, 11, 12, 13]. Nevertheless, MC methods require multiple model calls or training ensembles of models in parallel, leading to increased time and space complexity compared to deterministic models.

Approximating the distribution of a model's output up to its second order, the mean corresponds to the prediction, while the covariance corresponds to the prediction uncertainty. In this context, BVI supervises both the mean and covariance to ensure accurate predictions and reliable uncertainty estimation. However, we wonder whether the inherent non-linear coupling between the mean and covariance which has been observed in biological neuronal systems [14, 15] acts as a natural regulation for the covariance to capture the model's uncertainty. This raises the question of whether additional supervision for the covariance is necessary, and inspires us to construct a probabilistic computation framework in which we only supervise the mean and allow the covariance to emerge naturally through non-linear coupling with the mean. We propose that this "emerging covariance" provides a faithful representation of uncertainty.

The goal of this work is to develop a powerful and efficient framework of probabilistic computation. Our framework consists of a model called *moment neural network (MNN)* and a novel training procedure called *supervised mean and unsupervised covariance (SMUC)*. MNN conducts a stochastic network in a deterministic way via *moment activations (MAs)*, a class of simple activations capturing the non-linear transformation of mean and covariance across layers of the

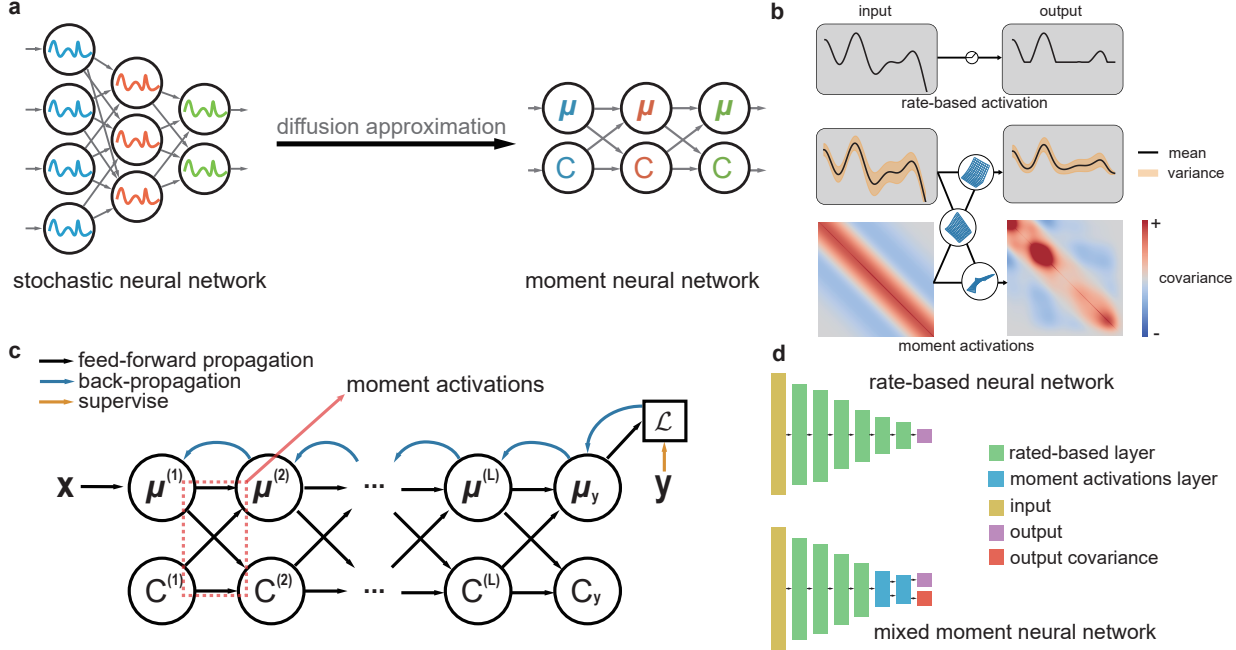


Figure 1: **Framework schematic.** **a**, Schematic of moment neural networks (MNNs). Left: stochastic feed-forward neural network (Eq. (6)). Right: MNNs (Eq. (5)). **b**, Comparison of rate-based activation and moment activations (MAs). We take the ReLU MAs as example. **c**, The MNNs and supervised mean unsupervised covariance (SMUC) training scheme. Different from rate-based neural networks, the feed-forward propagation of MNNs consists of both and mean and covariance. We train MNNs through SMUC, where the back-propagation only goes through the mean and taking the covariances as constants. **d**, The architecture of rate-based neural network (top) and mixed MNN (bottom). In the mixed MNN, the architecture retains the same layers as the rate-based neural network, with the exception that MAs are incorporated into the last few layers. The rectangles represent the layers, and their heights indicate the respective layer dimensions.

network. MNNs use linear combinations of MAs to learn complicated probabilistic representations, motivated by the universal approximation property of ANNs [16]. Instead of supervising both the mean and covariance, SMUC only conducts the back-propagation on the mean, and lets the covariance spontaneously emerge from the non-linear coupling with the mean. We demonstrate the theoretical equivalence of SMUC to stochastic Riemannian gradient descent [17], and highlight the exceptional capability of the emerging covariance for uncertainty quantification, out-of-distribution detection, and adversarial attack awareness. Our approach challenges the conventional perspective that uncertainty quantification requires supervision of the covariance. Instead, we show that when the model learns to predict labels based on the mean, the spontaneously emerging covariance becomes a reliable source for quantifying uncertainty, suggesting that probabilistic computation can be fundamentally simpler than previously believed.

Results

A. Probabilistic computation framework for supervised learning

Given samples of the input $\mathbf{x} \in \mathbb{R}^m$ and output (label) vector $\mathbf{y} \in \mathbb{R}^n$ pairs, we aim to learn a mapping $\mathbf{x} \mapsto q(\mathbf{y}|\mathbf{x})$ from a input \mathbf{x} to the probabilistic distribution of the prediction $q(\mathbf{y}|\mathbf{x})$, and quantify the prediction uncertainty by the entropy of $q(\mathbf{y}|\mathbf{x})$. Due to the inherent complexity, we propose constructing a Markov chain that decomposes this mapping into multiple probabilistic transition kernels, each of which may have a simpler form

$$\mathbf{x} \mapsto q(\mathbf{v}^{(1)}|\mathbf{x}) \mapsto q(\mathbf{v}^{(2)}|\mathbf{v}^{(1)}) \mapsto \dots \mapsto q(\mathbf{v}^{(L)}|\mathbf{v}^{(L-1)}) \mapsto q(\mathbf{y}|\mathbf{v}^{(L)}), \quad (1)$$

where $\mathbf{v}^{(l)}$ is the signal vector at l -th layer. Eq.(1) can be rewritten in terms of cumulant series [18]

$$\mathbf{x} \mapsto \{\boldsymbol{\mu}^{(1)}, \mathbf{C}^{(1)}, \dots\} \mapsto \{\boldsymbol{\mu}^{(2)}, \mathbf{C}^{(2)}, \dots\} \mapsto \dots \mapsto \{\boldsymbol{\mu}^{(L)}, \mathbf{C}^{(L)}, \dots\} \mapsto \{\boldsymbol{\mu}_y, \mathbf{C}_y, \dots\}, \quad (2)$$

where $\boldsymbol{\mu}^{(l)}, \mathbf{C}^{(l)}, \dots$ represent the mean, covariance matrix and higher order cumulants of the conditional distribution $q(\mathbf{v}^{(l)}|\mathbf{v}^{(l-1)})$, $\boldsymbol{\mu}_y$ is the prediction of \mathbf{y} , and \mathbf{C}_y is the prediction covariance. To ensure computability, we truncate

the cumulant series by considering only the first Z cumulants for each distribution and assuming that the higher-order cumulants beyond Z vanish. When $Z = 1$ as *deterministic computation*, the truncated process is written as

$$\mathbf{x} \mapsto \boldsymbol{\mu}^{(1)} \mapsto \boldsymbol{\mu}^{(2)} \mapsto \boldsymbol{\mu}^{(3)} \mapsto \cdots \mapsto \boldsymbol{\mu}^{(L)} \mapsto \boldsymbol{\mu}_y \quad (3)$$

We call Eq. (3) as *deterministic computation*, since the output is deterministic and the prediction entropy is always zero. We call the truncated process at $Z > 1$ as *probabilistic computation*, where two or higher order of cumulants account for the fluctuation and the uncertainty of the process. When $Z = 2$, the truncated process can be interpreted as a Gaussian process, where the transition of the mean and covariance at each layer expresses the evolution of the process

$$\mathbf{x} \mapsto \{\boldsymbol{\mu}^{(1)}, \mathbf{C}^{(1)}\} \mapsto \{\boldsymbol{\mu}^{(2)}, \mathbf{C}^{(2)}\} \mapsto \cdots \mapsto \{\boldsymbol{\mu}^{(L)}, \mathbf{C}^{(L)}\} \mapsto \{\boldsymbol{\mu}_y, \mathbf{C}_y\}. \quad (4)$$

We can calculate the entropy of the prediction distribution by considering it as a Gaussian distribution with mean $\boldsymbol{\mu}_y$ and covariance \mathbf{C}_y . When $Z > 2$, however, the truncated process can not be considered as a stochastic process due to the seminal result stating that the cumulant series of a probabilistic density function either has all but the first two terms vanish or has an infinite number of non-vanishing cumulants [18]. As a result, the entropy of the prediction distribution is undefined. Therefore, we select $Z = 2$ in our probabilistic computation framework. The remaining issue is to develop a learnable model for effectively conducting the truncated process devise a suitable training approach for this model.

B. Second-order approximation for stochastic networks

Inspired by the universal approximation theorem [16], which demonstrates that networks with simple non-linearity have the ability to approximate any continuous function, we consider a feed-forward stochastic neural network with element-wise non-linearity $\mathbf{h}(\cdot)$ and trainable parameters $W^{(l)}, \mathbf{b}^{(l)}$ (Eq. (6), [Methods](#)) for modeling $\mathbf{x} \mapsto q(\mathbf{y}|\mathbf{x})$, see the left of Fig. 1a for illustration. Next, we approximate the network up to its first two cumulants for constructing the truncated process Eq. (4) Drawing from a mathematically rigorous foundation, we can establish a set of non-linear mappings dubbed *moment activations* (MAs) $\mathbf{m}_v, \mathbf{C}_v$ (Eq. (7)-(8), [Methods](#)) describing how the neurons transfer the mean and covariance of received signals to that of the output signal. The exact expression of MAs depends on the function \mathbf{h} . We list MAs for Heaviside and ReLU function in [Methods](#), and call them as Heaviside and ReLU MAs respectively. As illustrated in Fig. 1b, MAs are the extension of rate-based activation, which only describes how neurons transfer the mean firing rate [19]. Incorporating MAs as the non-linearity, we introduce a class of neural network called *moment neural networks* (MNNs) to conduct the stochastic network (Eq. (6)) in a deterministic fashion (right of Fig. 1a)

$$\begin{aligned} \boldsymbol{\mu}^{(1)} &= \mathbf{x}, \quad \mathcal{C}^{(1)} = \sigma_1^2 \mathbf{I}, \\ \begin{cases} \bar{\boldsymbol{\mu}}^{(l)} = W^{(l-1)} \boldsymbol{\mu}^{(l-1)} + \mathbf{b}^{(l-1)}, \\ \boldsymbol{\mu}^{(l)} = \mathbf{m}_v(\bar{\boldsymbol{\mu}}^{(l)}, \bar{\mathcal{C}}^{(l)}), \end{cases} & \begin{cases} \bar{\mathcal{C}}^{(l)} = W^{(l-1)} \mathcal{C}^{(l-1)} (W^{(l-1)})^T + \sigma_l^2 \mathbf{I}, \\ \mathcal{C}^{(l)} = \mathbf{C}_v(\bar{\boldsymbol{\mu}}^{(l)}, \bar{\mathcal{C}}^{(l)}), \end{cases}, \quad l = 2, \dots, L \\ \boldsymbol{\mu}_y &= W^{(L)} \boldsymbol{\mu}^{(L)}, \quad \mathbf{C}_y = W^{(L)} \mathcal{C}^{(L)} (W^{(L)})^T. \end{aligned} \quad (5)$$

Rate-based neural network can be considered as a special case of MNN, where the covariances (blue part in Eq. (5)) are fixed at zero. We verify numerically that MNN well approximates the prediction mean and covariance of the stochastic network (Eq.(6)) ([Supplementary Information](#)). We also consider MAs derived from a biological neuronal model called leaky integrate-and-fire model [20] and investigate the corresponding MNN dubbed *LIF MNN* ([Supplementary Information](#)).

C. Training the stochastic network with unsupervised covariance

We train the MNN through a modified gradient descent algorithm called *supervised mean and unsupervised covariance (SMUC)* (Fig. 1c), where we only back-propagate the loss on the mean treating the covariances (blue part in Eq. (5)) as constants. As a result, the covariance spontaneously emerge through the non-linear coupling with the mean. The decision to only conducting back-propagation on the mean is not for computational efficiency. Rather, it brings following theoretical benefits (see [Supplementary Information](#) for proofs). First, SMUC is equivalent to stochastic Riemannian gradient descent [17] to fit the mean and variance for a ground-truth stochastic network. Second, under mild conditions, as the layer index l goes to infinity, the error in fitting the covariance matrix of the ground-truth stochastic network at the l -layer approaches zero (Eq. (S87), [Supplementary Information](#)). This observation suggests that as the depth of MNN increases, the accuracy of uncertainty quantification improves. Third, MNNs can take the low-dimension output of a rate-based neural network as its input, resulting in less computational cost on the calculating and storing the covariance matrices. We call this model as *mixed MNN* (Fig. 1d). The training complexity of MNNs can be further reduced by using the batch-wise covariance trick with only marginal reduction in performance ([Supplementary Information](#)).

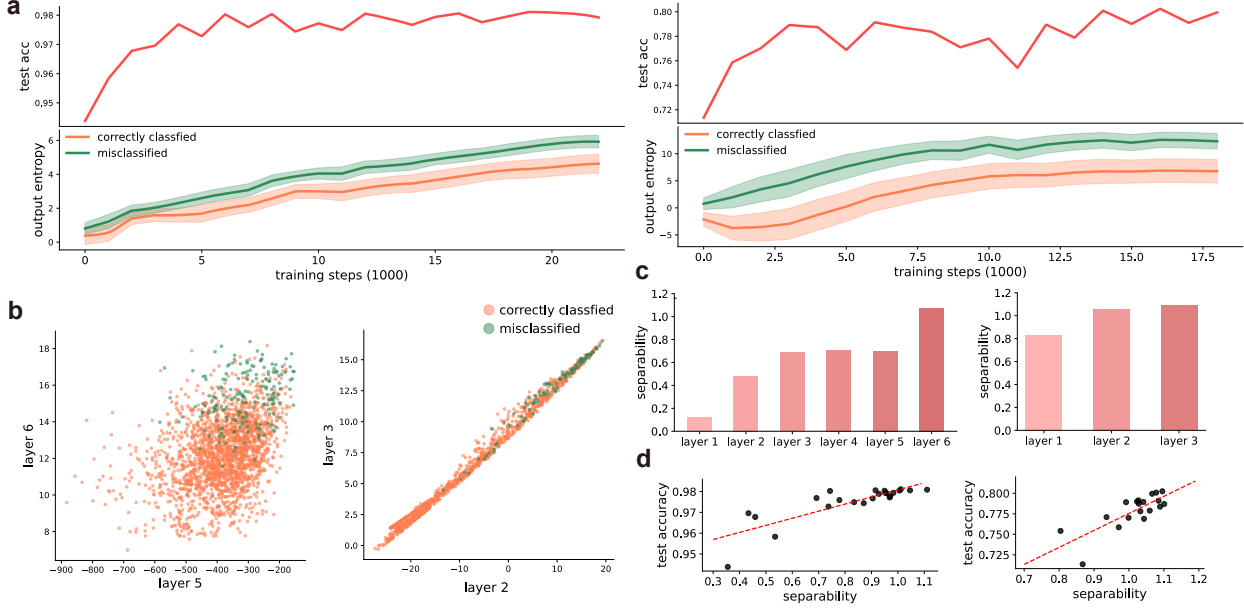


Figure 2: Emerging covariance faithfully captures the prediction uncertainty. (Mixed) ReLU MNN trained on MNIST (CIFAR-10) for image classification. Consistent results are observed in Heaviside and LIF MNNs (Fig. S8, Fig. S1, [Supplementary Information](#)). **a**, Training MNNs on MNIST (left) and CIFAR-10 (right), with the accuracy (red line) and entropy (orange and green for correctly classified inputs and misclassified inputs respectively) on the test set. The shadows indicate the level of half standard deviations. **b**, The entropy of correctly classified and misclassified inputs in the last two layers of MNIST (left) and CIFAR-10 (right). **c**, The entropy separability of correctly classified and misclassified inputs on MNIST (left) and CIFAR-10 (right) increases as the layer index increases. **d**, Linear regression on the separability and test accuracy during training on MNIST (left) and CIFAR-10 (right). The red dashed line represents the regression line, with coefficients of determination of 0.6803 for MNIST and 0.6068 for CIFAR-10.

D. Emerging covariance faithfully captures uncertainty

We calculate the *entropy* ([Methods](#)) of the output distribution $\mathcal{N}(\mathbf{m}_y, C_y)$ as quantification of the prediction uncertainty. We train a full-connected MNN on MNIST [21] and record the classification accuracy and the entropy on the test set across the training procedure (Fig. 2a). As the training progresses, the model exhibits higher uncertainty on misclassified inputs compared to correctly classified ones, indicating that entropy can effectively quantify the model's uncertainty, with higher values indicating lower confidence. We calculate the *separability* ([Methods](#)) of entropy across layers between correctly and misclassified inputs to evaluate the statistical difference of entropy on misclassified and correctly classified samples (Fig. 2c). As the layer index increases, the separability also increases, indicating that the covariance estimation is more accurately with deeper layers, collaborating the theoretical result (Eq. (S85)). While it is well known that increasing the depth of a neural network improves its function fitting ability [22], our finding presents another perspective: deeper networks enable more accurate uncertainty estimations. We also find that there is a considerably positive correlation between the separability and accuracy on the test set across the training procedure (Fig. 2d), suggesting that the performance of prediction and uncertainty quantification are positively correlated. Consistent results are observed in the mixed MNNs trained on CIFAR-10 [23] (Fig. 2).

To investigate whether the entropy of MNNs can indicate high uncertainty on out-of-distribution (OOD) samples, we train an MNN on MNIST, and treat the samples in the notMNIST [24] as the OOD inputs. As shown in Fig. 3a and b, the entropy is the most reliable indicator for separating the correctly classified, misclassified and OOD samples compared to *maximum softmax probability* (*MSP*) and *softmax entropy* (*SE*) [25], two OOD indicators calculated from the prediction mean ([Methods](#)). This implies that the covariance are a more proper source of uncertainty estimation than the mean. It is plausible that *MSP* and *SE* can still offer valuable information about uncertainty, since the mean and covariance are non-linearly coupled, and they may share some common information regarding uncertainty.

We investigate the potential of MNNs to defend against gradient-based adversarial attacks [26, 27], which can significantly decrease the performance of classifiers by imperceptibly modifying the input. We apply fast gradient sign method (FGSM) [27] to generate adversarial samples. We first train an Heaviside MNN on MNIST dataset, and "turn

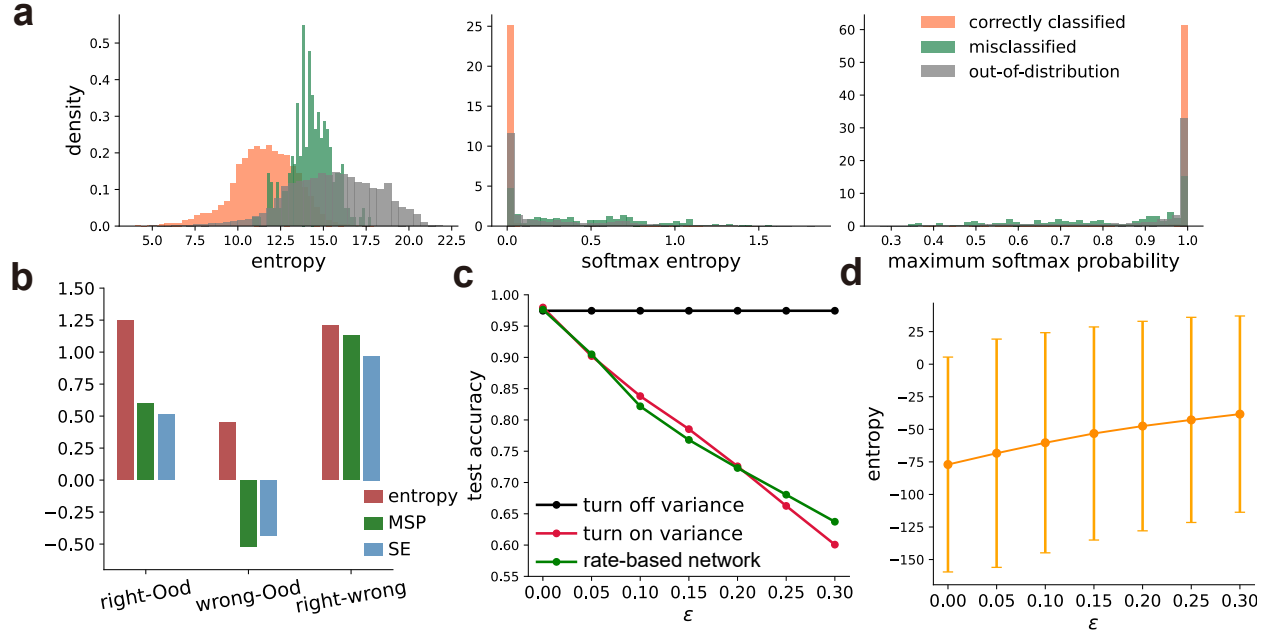


Figure 3: MNNs for OOD detection and adversarial attack defense and awareness. **a**, The distribution of entropy, MSP, and SE on correctly classified, misclassified and OOD input. **b**, The separability of three indicators on the correctly classified (denoted as 'right'), misclassified (denoted as 'wrong') and OOD samples. The negative value of separability implies that the MSP and SE incorrectly indicate higher uncertainty for misclassified samples compared to OOD samples. **c**, The test accuracy of rate-based network, MNN conducted with and without turn-off variance under different strength ϵ of FGSM attacks. **d**, The average entropy of the samples in the test set calculated by the MNN implemented without turn-off variance under different strength ϵ of FGSM attacks.

off variance" by setting σ_1, σ_2 (Eq. (5)) to zero, making the first layer of MAs degenerate into the Heaviside function. After turn-off variance, the FGSM attack has no effect on this model in Fig. 3c, since the gradient of model is always zero, while there is only marginal drop on the test accuracy (from 0.9797 to 0.9745). Without turn-off variance, the MNN is vulnerable to the adversarial attack (Fig. 3c). Nevertheless, the MNN now is aware of the attack in terms of the increasing of the entropy (Fig. 3d).

E. Interpreting the uncertainty represented by the emerging covariance

To understand why misclassified and adversarial inputs result in high entropy, we train an MNN for a binary classification problem ([Methods](#)) as shown in (Fig. 4a). Since the model fits well with the dataset (Fig. 4b), we consider the classification boundary as the decision boundary learned by the model. It is observed that for an input x , the lower its distance to the decision boundary (x_1 and x_2 axes), the higher the output entropy is (Fig. 4c). Noticed that inputs that are located closer to the decision boundaries exhibit higher sensitivity, as small perturbations can move them across the boundaries. Therefore, the distance to the decision boundary is inherently linked to the sensitivity. MNNs capture this sensitivity by propagating stochastic fluctuations in each layer to the output. Inputs that exhibit higher sensitivity to the output result in larger variations in the output covariance, leading to higher output entropy (see [Supplementary Information](#) for a theoretical illustration). Since misclassified and adversarial inputs are often near the decision boundary [28], their entropy are relatively higher.

We further investigate why the OOD samples result in high entropy. We train an MNN on a binary classification problem ([Methods](#)) and observe that OOD samples exhibit higher entropy compared to in-distribution samples (Fig. 4d,e). Additionally, we discover that samples closer to the boundary of the training set tend to have higher entropy (Fig. 4f). According to the analysis in the last paragraph, high entropy samples can serve as an detector of the decision boundaries with samples closer to the decision boundary displaying higher entropy. This leads us to formulate the following interpretative hypothesis. Initially, decision boundaries of the model are randomly distributed across the input space. During training, the model adapts the decision boundaries to fit the training data, resulting in relatively sparse boundaries that align with the data distribution. However, in the OOD region, the absence of label guidance results in a lack of

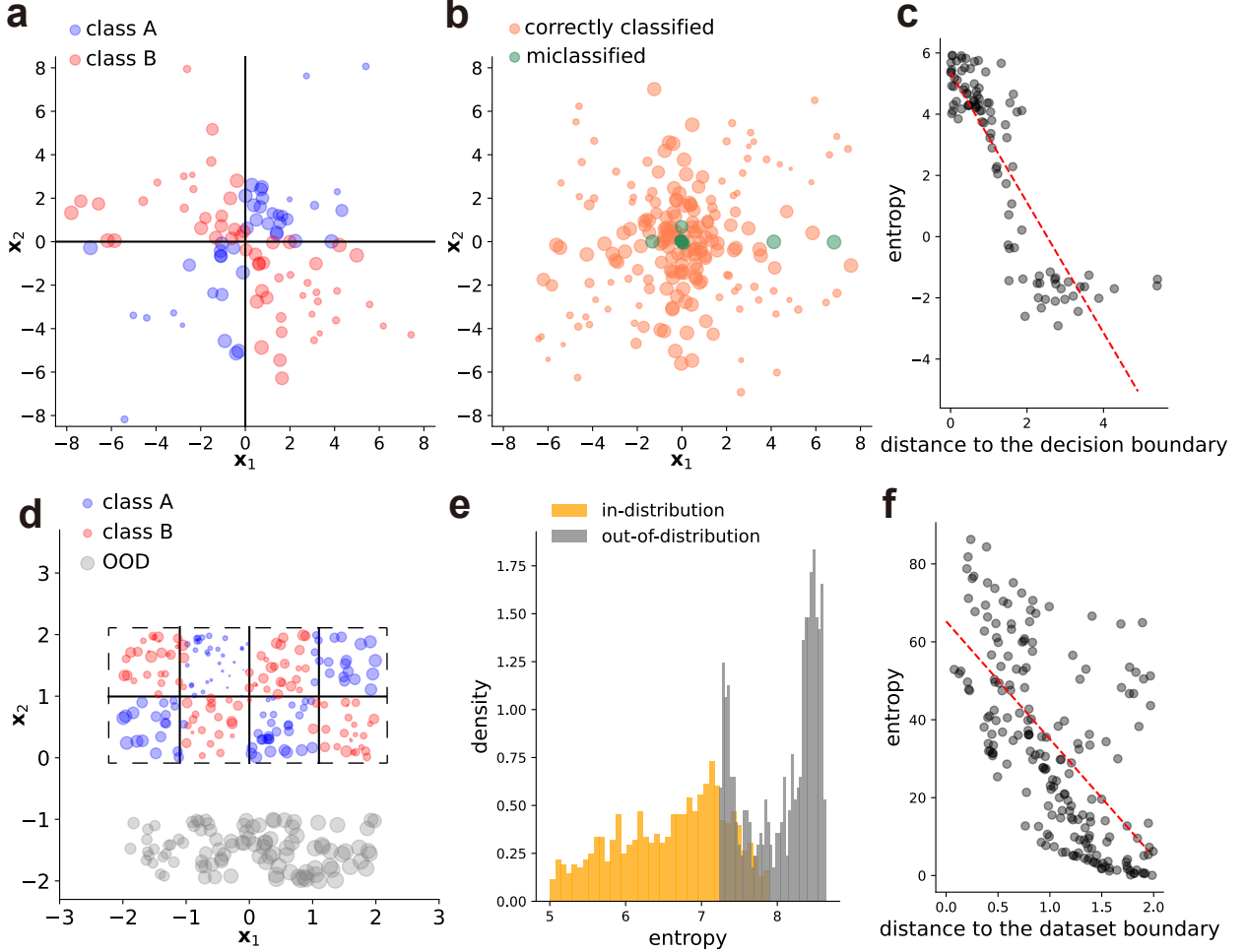


Figure 4: Interpreting the uncertainty captured by the emerging covariance. **a**, An MNN is trained on a binary classification problem on \mathbb{R}^2 , where the two classes indicated by blue and red bubbles, and the classification boundary is indicated by the solid lines. The size of bubbles indicates how large the output entropy is. **b**, The MNN in **a** reaches classification accuracy of 0.9948, hence the decision boundary learned by the model fits well with the classification boundary of the dataset. **c**, For samples in **a**, the distance to the decision boundary is negatively correlated with the entropy (coefficient of determination is 0.7196). **d**, An MNN is trained on another binary classification problem on \mathbb{R}^2 . The two classes are indicated by blue and red bubbles, the OOD samples are indicated by grey bubbles, the classification boundary is indicated by the solid lines, and the boundary of the training dataset (in-distribution region) is indicated by the dashed line. **e**, For samples in **d**, the entropy of the OOD samples (grey) are higher than that of the in-distribution samples (yellow). **f**, For in-distribution samples in **d**, the distance to the training dataset boundary is negatively correlated with the entropy (coefficient of determination is 0.4296).

structured boundaries, leading to a relatively dense distribution of decision boundaries. As a result, the entropy of OOD samples tends to be higher compared to that of in-distribution samples.

Discussion

In the pursuit of artificial general intelligence (AGI), probabilistic computation approaches become crucial to enable models to incorporate uncertainty in a manner that emulates human reasoning [29]. However, this remains a challenging task due to the computational complexity involved. Our work introduces two novel ingredients for probabilistic computation, thereby expanding its applicability and scalability.

First, we manage to use simple non-linearities (MAs, Eq. (7)-(8)) to learn complex probabilistic representation in a closed form, inheriting the spirit of the universal approximation theory that facilitates fitting deterministic functions

using simple non-linearities. We construct a deterministic neural network (MNN, Eq. (5)) using MAs to approximate a parameterized stochastic neural network (Eq. (6)) up to its second cumulants. MNNs efficiently calculate the mean and covariance of a stochastic network in a single pass, enabling direct gradient descent optimization for training, rather than relying on Monte Carlo methods which can be computationally expensive. Moreover, MNNs offer a unique advantage in analyzing the dynamics of stochastic networks by explicitly expressing the non-linear coupling between the mean and covariance. This coupling is implicit in Monte Carlo methods, and can be difficult to analyze directly.

Second, we provide new insights into how a model learns to incorporate uncertainty in its predictions. It is reasonable in a traditional perspective to supervise both the prediction and the prediction uncertainty during training, as a model may excel in making predictions but falter in evaluating the uncertainty of those predictions. A well-known example is BVI (Eq. (S117), [Supplementary Information](#)), the current popular probabilistic computation approach. We challenge this view by proposing our training method (SMUC, Eq. (5)-(23)), which back-propagates the loss only on the mean while taking the covariance as constants during gradient descent, and reveal that the covariance spontaneously emerging from the non-linear coupling with the mean can be harnessed for effective uncertainty quantification without supervising (Fig. 2-3). This finding distinguishes our work from BVI, which we categorize as supervising both the mean and covariance (SMSC). To gain insights into how the emerging covariance is able to capture the uncertainty, we conducted extra experiments (Fig. 4) and theoretical derivation ([Supplementary Information](#)) to demonstrate that the output uncertainty captures the sensitivity of the network, resulting in high entropy on misclassified, attacked and OOD samples. Additionally, we proved theoretically that MNN can learn the mean and variance of the ground-truth stochastic network, and the error on covariance is reduced to zero as the layer number goes to infinity under mild conditions ([Supplementary Information](#)), enabling the MNN to faithfully capture uncertainty akin to the stochastic network [30].

Our work also offers a hypothesis for the learning rules employed by the brain. We expect that although neural computation in biological systems is inherently probabilistic due to the presence of various sources of noise and variability [31], the learning process can be realized by adjusting synapses through gradient descent on the mean firing rate of neurons. In this gradient descent process, the neural fluctuations are treated as constant, and only the loss on the mean firing rate is back-propagated, similar to SMUC. Our hypothesis is founded on three key factors: first, we have demonstrated that the MNN derived from leaky integrate-and-fire (LIF) model also exhibits the same ability to capture prediction uncertainty (Fig. S1, [Supplementary Information](#)), while the LIF model is widely applied for modeling the neuronal circuit in the brain. second, experimental studies on biological neural systems, especially in sensory systems, have revealed that neurons code information through their mean firing rates [32, 33]; third, it is commonly hypothesized that the brain adjusts synapses in a manner similar to gradient descent [34]; To further empirically validate this hypothesis, we propose investigating whether other neural dynamics or task behaviors observed in the brain can be replicated by stochastic networks trained using gradient-based algorithms, similar to the study by [35] which demonstrated that gradient-based models were able to replicate human patterns of sensitivity. Future studies could focus on investigating whether our framework can successfully replicate properties of neural dynamics at the individual neuron level observed in the brain, as documented in studies such as [36].

Approximating the stochastic network up to its first two cumulants is justified by empirical evidence and theoretical analysis. In [37], the authors analyzed neural data of vertebrate retina and discovered that the pairwise correlations of biological networks can make accurate predictions of the collective effects of the system without considering higher-order interactions. In [38], the authors examined higher-order cumulants and discovered that in a weakly correlated state, the contributions of higher-order cumulants on network dynamics are significantly smaller, implying that the first two cumulants provide a reasonably accurate representation of the network dynamics.

Studies have shown that noise is not merely a hindrance to neural system, but can also play functional roles [39, 40]. Our findings suggest that noise enables the model to become aware of its own uncertainty. Furthermore, noise enables us to train a network using gradient descent even when the activation gradients vanish, which is inherently immune to gradient-based adversarial attacks (left of Fig. 3c). This also suggests an alternative strategy for training a network whose gradient vanishes, different from the surrogate loss [41] used for training spike neural networks.

Several BVI methods [42, 43, 44, 45] represent the stochasticity of neural networks in a deterministic fashion, similar to MNNs. The primary difference between MNNs and these methods is that the latter belong to the category of SMSC. Additionally, MNNs estimate the covariance using linear response theory [46], while these methods rely on asymptotic approximations [44]. Moreover, these methods introduce stochasticity to the weight of the network, whereas MNNs incorporate stochasticity in the state of each layer and biases. We compare MNNs with these methods and show better performance in both regression and classification tasks ([Supplementary Information](#)).

In unsupervised learning, where labels are unavailable, it is possible to supervise the covariance for representation learning. An example is the Barlow Twins method [47] for self-supervised learning, where an encoder is trained using a covariance-based loss function to reduce redundancy. This suggests that we have the potential to train MNNs using the unsupervised mean and supervised covariance (UMSC) approach for unsupervised learning tasks.

Methods

Moment activations (MAs)

We consider a feed-forward stochastic neural network with element-wise non-linearity $\mathbf{h}(\cdot)$, which transfers each coordinate \mathbf{x}_i through a real function $h_i(\mathbf{x}_i)$

$$\begin{aligned}\frac{d\mathbf{x}^{(1)}}{dt} &= -\mathbf{x}^{(1)} + \mathbf{x} + \sqrt{2}\sigma^{(1)}\boldsymbol{\xi}^{(1)}, \quad \mathbf{v}^{(1)} = \mathbf{x}^{(1)} \\ \frac{d\mathbf{x}^{(l)}}{dt} &= -\mathbf{x}^{(l)} + W^{(l-1)}\mathbf{v}^{(l-1)} + \mathbf{b}^{(l-1)} + \sqrt{2}\sigma_l\boldsymbol{\xi}^{(l)}, \quad \mathbf{v}^{(l)} = \mathbf{h}(\mathbf{x}^{(l)}), \quad l = 2, \dots, L \\ \frac{d\mathbf{y}}{dt} &= -\mathbf{y} + W^{(L)}\mathbf{v}^{(L)},\end{aligned}\tag{6}$$

where $\mathbf{x}^{(l)}$ are the neural state, $\mathbf{v}^{(l)}$ are the signals transmitted to neurons at the next layer, $W^{(l)}, \mathbf{b}^{(l)}$ are the learnable weights and biases, $\boldsymbol{\xi}^{(l)}$ are standard Brownian motions, and $\sigma_l > 0$ are constants. In general, it is hard to solve $\mathbf{v}^{(l)}$ analytically. Nevertheless, under steady-state distribution, we can approximate $\mathbf{v}^{(l)}$ by a Gaussian distribution $\mathcal{N}(\bar{\mu}^{(l)}, \bar{C}^{(l)})$ using diffusion approximation [48, 49] (Supplementary Information), and then the signals received by the neurons at l -th layer obey a Gaussian distribution $\mathcal{N}(\bar{\mu}^{(l)}, \bar{C}^{(l)})$, with $\bar{\mu}^{(l)} = W^{(l-1)}\boldsymbol{\mu}^{(l-1)} + \mathbf{b}^{(l-1)}$ and $\bar{C}^{(l)} = W^{(l-1)}C^{(l-1)}(W^{(l-1)})^T + \sigma_l^2 I$. Based on the linear response theory [46] (Supplementary Information), we obtain a set of non-linear mappings dubbed *moment activations* (MAs) describing how the neurons transfer the first two moments of received signals to that of the output signal

$$\mu_i = (\mathbf{m}_v(\bar{\mu}, \bar{C}))_i = m_{v,i}(\bar{\mu}_i, \bar{C}_i),\tag{7}$$

$$C_{ij} = (C_v(\bar{\mu}, \bar{C}))_{ij} = \begin{cases} C_{v,i}(\bar{\mu}_i, \bar{C}_i), & i = j \\ \chi_i(\bar{\mu}_i, \bar{C}_i)\chi_j(\bar{\mu}_j, \bar{C}_j)c_{ij}, & i \neq j \end{cases}\tag{8}$$

where $c_{ij} = \frac{\bar{C}_{ij}}{\sqrt{\bar{C}_i\bar{C}_j}}$ is the correlation coefficient. We list two instantiations of the MAs used the main paper, and put the MAs derived from leaky integrate-and-fire neuronal model in Supplementary Information. See Supplementary Information for the derivation of the MAs (Eq. (S21), (S22), and (S25)).

Heaviside function. When all the signal functions h_i are Heaviside function

$$h(x) = \begin{cases} 1, & x \geq 0 \\ 0, & x < 0 \end{cases},\tag{9}$$

the corresponding MAs are

$$m_v(\bar{\mu}, \bar{C}) = \frac{1}{2} + \frac{1}{\sqrt{2\pi}} \int_0^{\frac{\bar{\mu}}{\sqrt{\bar{C}}}} e^{-\frac{x^2}{2}} dx,\tag{10}$$

$$C_v(\bar{\mu}, \bar{C}) = \frac{1}{2} + \frac{1}{\sqrt{2\pi}} \int_0^{\frac{\bar{\mu}}{\sqrt{\bar{C}}}} e^{-\frac{x^2}{2}} dx - \left(\frac{1}{2} + \frac{1}{\sqrt{2\pi}} \int_0^{\frac{\bar{\mu}}{\sqrt{\bar{C}}}} e^{-\frac{x^2}{2}} dx\right)^2,\tag{11}$$

$$\chi(\bar{\mu}, \bar{C}) = \frac{1}{\sqrt{2\pi}} \exp\left(-\frac{\bar{\mu}^2}{2\bar{C}}\right).\tag{12}$$

ReLU function. When all the signal functions h_i are ReLU function

$$h(x) = \begin{cases} x, & x \geq 0 \\ 0, & x < 0 \end{cases},\tag{13}$$

the corresponding MAs are

$$m_v(\bar{\mu}, \bar{C}) = \frac{\sqrt{\bar{C}}}{\sqrt{2\pi}} \exp\left(-\frac{\bar{\mu}^2}{2\bar{C}}\right) + \bar{\mu}\left(\frac{1}{2} + \frac{1}{\sqrt{2\pi}} \int_0^{\frac{\bar{\mu}}{\sqrt{\bar{C}}}} e^{-\frac{x^2}{2}} dx\right),\tag{14}$$

$$C_v(\bar{\mu}, \bar{C}) = (\bar{C} + \bar{\mu}^2)\left(\frac{1}{2} + \frac{1}{\sqrt{2\pi}} \int_0^{\frac{\bar{\mu}}{\sqrt{\bar{C}}}} e^{-\frac{x^2}{2}} dx\right) + \frac{\bar{\mu}\sqrt{\bar{C}}}{\sqrt{2\pi}} \exp\left(-\frac{\bar{\mu}^2}{2\bar{C}}\right) - m_v(\bar{\mu}, \bar{C})^2,\tag{15}$$

$$\chi(\bar{\mu}, \bar{C}) = \frac{\sqrt{\bar{C}} + \bar{\mu}}{\sqrt{2\pi}} \exp\left(-\frac{\bar{\mu}^2}{2\bar{C}}\right) + \sqrt{\bar{C}}\left(\frac{1}{2} + \frac{1}{\sqrt{2\pi}} \int_0^{\frac{\bar{\mu}}{\sqrt{\bar{C}}}} e^{-\frac{x^2}{2}} dx\right).\tag{16}$$

We can also consider the heterogenous case, where different neurons apply different signal functions, and the covariance activation at that case is $\chi_i \chi_j c_{ij}$, where the form of χ_i depends on the signal function of the i -th neuron.

The covariance mapping derived above has a strong connection to the result for LIF neuronal model [46]. To reveal this, note that

$$\frac{\partial}{\partial \bar{\mu}} m_v(\bar{\mu}, \bar{C}) = \frac{1}{\sqrt{\bar{C}}} \chi(\bar{\mu}, \bar{C}), \quad (17)$$

hence the covariance can be written as

$$\frac{\partial}{\partial \bar{\mu}_i} m_{v,i}(\bar{\mu}_i, \bar{C}_i) \frac{\partial}{\partial \bar{\mu}_j} m_{v,j}(\bar{\mu}_j, \bar{C}_j) \sqrt{\bar{C}_i \bar{C}_j} c_{ij}. \quad (18)$$

However, the covariance of the input signals is $2\sqrt{\bar{C}_i \bar{C}_j} c_{ij}$ (see Eq. (S17)), instead of $\sqrt{\bar{C}_i \bar{C}_j} c$. Therefore, there is a difference of factor 2 between results of our covariance activation and the one induced in [46]. The difference arises because, in the latter case, the linear response theory is used for estimating coherence, which corresponds to the correlation coefficient of two output signals in the frequency domain. Conversely, in the former case, the linear response theory is used for estimating the correlation coefficient of the two output signals (in the time domain). When h_i are all linear, the coherence measure is twice the correlation coefficient of the output signals.

Metrics

Entropy. The output of the MNN is a multi-dimensional Gaussian distribution $\mathcal{N}(\mu_y, C_y)$, and we calculate the entropy as

$$H(\mathcal{N}(\mu_y, C_y)) = \frac{n}{2}(1 + \log 2\pi) + \frac{1}{2} \log \det[C_y], \quad (19)$$

where n is the dimension of the output. It is important to note that the entropy indicators do not incorporate the output mean μ_y , which is supervised during training. Instead, these indicators solely rely on the output covariance C_y , which emerges from the non-linear coupling with the first moment in the MNN. Additionally, we can calculate the entropy at any layer of the MNN. Given the moments of the l -th layer as $\mathcal{N}((\mu_v^{(l)}, C_v^{(l)}))$, the entropy is

$$H(\mathcal{N}(\mu_v^{(l)}, C_v^{(l)})) = \frac{m^{(l)}}{2}(1 + \log 2\pi) + \frac{1}{2} \log \det[C_v^{(l)}], \quad (20)$$

If C_y is singular, we have $\det[C_y] = 0$, which leads to infinity small entropy. In such scenarios, we compute the entropy in the subspace where the covariance matrix C_y is full-rank. To achieve this, we calculate the determinant of C_y using singular value decomposition (SVD). Instead of using the actual dimension, we consider the number of positive singular values of C_y as the effective dimension for the entropy calculation.

Separability. Suppose we aim to quantify the degree of separation for a variable between two populations, labeled as 1 and 2. In such cases, we can calculate the separability metric as

$$\frac{\mu_1 - \mu_2}{\sqrt{\sigma_1^2 + \sigma_2^2}}, \quad (21)$$

where μ_1 and μ_2 are the means of the variable in population 1 and 2 respectively, and σ_1^2 and σ_2^2 are variances of the variable in population 1 and 2 respectively. A higher absolute value of the separability indicates a greater statistical distinction between the two populations.

Maximum softmax probability (MSP) and softmax entropy (SE). Given the model output mean μ_y , we can define a probabilistic distribution using softmax function

$$p_i = \frac{\exp\{\mu_{y,i}\}}{\sum_{j=1}^n \exp\{\mu_{y,j}\}}, \quad i = 1, \dots, n. \quad (22)$$

The Maximum softmax Probability (MSP) has been widely employed as an indicator for detecting out-of-distribution samples [25]. The MSP is determined by calculating the maximum probability, denoted as $\max_i p_i$, from the softmax output. Lower values of MSP indicate higher uncertainty in the model's predictions. Another indicator is the entropy of the distribution $\{p_i\}$ [50], calculated as $-\sum_{i=1}^n p_i \log p_i$. We call this entropy as softmax entropy (SE), to distinguish it from the entropy calculated by MNNs.

Another indicator utilized is the entropy of the distribution p_i , as proposed by [50]. The entropy, referred to as softmax entropy (SE) in this context, is computed as $-\sum_{i=1}^n p_i \log p_i$. It is important to distinguish this entropy from the entropy calculated by MNNs. The SE provides a measure of the uncertainty in the softmax output distribution. Higher SE values indicate greater uncertainty in the model's predictions.

Training implementations

Given input-output pairs (\mathbf{x}, \mathbf{y}) from the dataset \mathcal{D} , the task loss function \mathcal{L} , and learning rate γ_t , we update the parameters $\theta = \{W^{(l)}, \mathbf{b}^{(l)}\}$ of the MNN through the *supervised mean and unsupervised covariance (SMUC)*

$$\theta_{t+1} = \theta_t - \gamma_t \sum_{(\mathbf{x}, \mathbf{y}) \in \mathcal{D}} \frac{\partial \mathcal{L}(\mathbf{y}, \mu_y(\mathbf{x}, \theta_t))}{\partial \theta_t}, \quad (23)$$

where we only back-propagate the loss on the mean treating the second moments. By default, we utilize the cross-entropy loss function as the objective function and employ the Adam optimizer [51] for training, without any additional specifications. Additionally, we set σ_l to a value of 0.2 for all layers.

Classification on MNIST [23]. We train a ReLU MNN, whose architecture consisting of six fully connected layers with dimensions of 784, 392, 196, 96, 48, 24, 10, respectively. We set the training batch size as 128, the learning rate as 0.0005, weight decay factor as 0.001 and the training epochs as 50.

Classification on CIFAR-10 [23]. We train a mixed MNN with ReLU MAs. The network consists of 10 layers of convolutional layer. The construction of these convolutional layers follows the design of VGG13 [52]. After the convolutional layers, three MA layers are connected. The dimensions of these layers are set as 64, 32, 10, respectively. We set the training batch size as 128, the learning rate as 0.0005, weight decay factor as 0.001 and the training epochs as 120, using random crop and random horizontal flip as data augmentation.

Out-of-distribution detection. We train a full-connected ReLU MNN on the MNIST dataset, and the dimension of each layer is 784, 392, 196, 96, 48, 24, 10. The training batch-size is 128, and epoch is 50, the learning rate is 0.0005, and the factor of weight decay is 0.0001. After training, we use the notMNIST [24] dataset as the out-of-distribution samples. NotMNIST dataset consists of 28×28 grayscale images of alphabets from A to J .

Adversarial attack defense and awareness. For adversarial attack experiment, we train an fully-connected Heaviside MNN on MNIST, where the dimension of each layer is 784, 392, 196, 96, 48, 24, 10. The training batch-size is 128, and epoch is 50, the learning rate is 0.0005, and the factor of weight decay is 0.0001. We apply the fast gradient sign method (FGSM) [27] for generating adversarial samples on the test set. FGSM adds an optimal max-norm constrained perturbation to the input \mathbf{x} , and this perturbation is calculated as

$$\epsilon \text{sgn}(\nabla_{\mathbf{x}} \mathcal{L}(\theta, \mathbf{x}, \mathbf{y})), \quad (24)$$

where \mathbf{x}, \mathbf{y} is an input-output pair from dataset, θ is the parameters of the trained model, and $\epsilon > 0$ controls the strength of the perturbation. The FGSM finds the direction along which the model output changes the most and adds small perturbation along that direction.

Binary classification problem for Fig. 4a,b. Given input $\mathbf{x} \in \mathbb{R}^2$, it belongs to class A if the sign of two coordinates $\mathbf{x}_1, \mathbf{x}_2$ are the same, otherwise it belongs to class B. In other words, $\mathcal{A} = \{\mathbf{x} \in \mathbb{R}^2, \mathbf{x}_1 \mathbf{x}_2 > 0\}$, and $\mathcal{B} = \{\mathbf{x} \in \mathbb{R}^2, \mathbf{x}_1 \mathbf{x}_2 < 0\}$. The decision boundaries are $\{\mathbf{x} \in \mathbb{R}^2, \mathbf{x}_1 = 0\}$ and $\{\mathbf{x} \in \mathbb{R}^2, \mathbf{x}_2 = 0\}$. We train a fully-connected ReLU MNN. The dimensions of each layer in the network are 2, 64, 32, 16, 8, 2, respectively, and σ_l are all set as 0.5. We generate the training set of 10,000 samples by randomly sampling from a standard Gaussian distribution on \mathbb{R}^2 . The training batch is 128, the epoch is 20, the learning rate is 0.0005, and the factor of the weight decay is 0.00001.

Binary classification problem for Fig. 4c,d,e. The the in-distribution (training) set is $\mathcal{D}_x = \{\mathbf{x} \in \mathbb{R}^2, \mathbf{x}_1 \in (-2, 2), \mathbf{x}_2 \in (0, 2)\}$. The set of class A is

$$\mathcal{A} = \mathcal{D}_x \cap ((-2, -1) \times (0, 1) \cup (-1, 0) \times (1, 2) \cup (0, 1) \times (0, 1) \cup (1, 2) \times (1, 2)), \quad (25)$$

and the set of class B is

$$\mathcal{B} = \mathcal{D}_x \cap ((-2, -1) \times (1, 2) \cup (-1, 0) \times (0, 1) \cup (0, 1) \times (1, 2) \cup (1, 2) \times (0, 1)). \quad (26)$$

We train a fully-connected ReLU MNN. The dimensions of each layer in the network are 2, 512, 256, 128, 64, 2, respectively, and σ_l are all set as 1. The samples uniformly distributed in the range $(-2, 2) \times (-2, -1)$ are considered as the OOD samples. We generate the training set of 20,000 samples by randomly sampling from the uniform distribution on \mathbb{R}^2 . The training batch is 32, the epoch is 10, the learning rate is 0.0001, and the factor of the weight decay is 0.001.

Code Availability

The code for training the moment neural network (MNN) through supervised mean and unsupervised covariance (SMUC) is available without restrictions on GitHub (<https://github.com/AwakerMhy/probabilistic-computing-mnn>).

Acknowledgments

Supported by STI2030-Major Projects (No. 2021ZD0200204); supported by Shanghai Municipal Science and Technology Major Project (No. 2018SHZDZX01), ZJ Lab, and Shanghai Center for Brain Science and Brain-Inspired Technology; supported by the 111 Project (No. B18015).

Author Contributions

Conceptualization: H.M. and J.F.; Methodology: H.M., Y.Q., W.L. and J.F.; Investigation: H.M. and Y.Q.; Software: H.M.; Visualization: H.M.; Writing — original draft: H.M.; Writing — review & editing: H.M., Y.Q., L.Z., W.L., and J.F.; Supervision: J.F.

Competing interests

The authors declare no competing interests.

Materials & Correspondence

Correspondence and requests for materials should be addressed to J.F.

References

- [1] John Von Neumann and Ray Kurzweil. *The computer and the brain*. Yale university press, 2012.
- [2] Ben Goertzel. Human-level artificial general intelligence and the possibility of a technological singularity: A reaction to ray kurzweil's the singularity is near, and mcdermott's critique of kurzweil. *Artificial Intelligence*, 171(18):1161–1173, 2007.
- [3] Zoubin Ghahramani. Probabilistic machine learning and artificial intelligence. *Nature*, 521(7553):452–459, 2015.
- [4] Moloud Abdar, Farhad Pourpanah, Sadiq Hussain, Dana Rezazadegan, Li Liu, Mohammad Ghavamzadeh, Paul Fieguth, Xiaochun Cao, Abbas Khosravi, U Rajendra Acharya, et al. A review of uncertainty quantification in deep learning: Techniques, applications and challenges. *Information Fusion*, 76:243–297, 2021.
- [5] Dominik Seuß. Bridging the gap between explainable ai and uncertainty quantification to enhance trustability. *arXiv preprint*, 2021.
- [6] Michael I Jordan, Zoubin Ghahramani, Tommi S Jaakkola, and Lawrence K Saul. An introduction to variational methods for graphical models. *Machine learning*, 37:183–233, 1999.
- [7] Arnaud Doucet, Nando De Freitas, Neil James Gordon, et al. *Sequential Monte Carlo methods in practice*. Springer, 2001.
- [8] John Paisley, David Blei, and Michael Jordan. Variational bayesian inference with stochastic search. *arXiv preprint*, 2012.
- [9] Diederik P Kingma and Max Welling. Auto-encoding variational bayes. *arXiv preprint*, 2013.
- [10] Yarin Gal and Zoubin Ghahramani. Dropout as a bayesian approximation: Representing model uncertainty in deep learning. In *international conference on machine learning*, pages 1050–1059. PMLR, 2016.
- [11] Mattias Teye, Hossein Azizpour, and Kevin Smith. Bayesian uncertainty estimation for batch normalized deep networks. In *International Conference on Machine Learning*, pages 4907–4916. PMLR, 2018.
- [12] Aryan Mobiny, Pengyu Yuan, Supratik K Moulik, Naveen Garg, Carol C Wu, and Hien Van Nguyen. Dropconnect is effective in modeling uncertainty of bayesian deep networks. *Scientific reports*, 11(1):1–14, 2021.
- [13] Balaji Lakshminarayanan, Alexander Pritzel, and Charles Blundell. Simple and scalable predictive uncertainty estimation using deep ensembles. *Advances in neural information processing systems*, 30, 2017.
- [14] Adrián Ponce-Alvarez, Alexander Thiele, Thomas D Albright, Gene R Stoner, and Gustavo Deco. Stimulus-dependent variability and noise correlations in cortical mt neurons. *Proceedings of the National Academy of Sciences*, 110(32):13162–13167, 2013.
- [15] Stefano Panzeri, Monica Moroni, Houman Safaai, and Christopher D Harvey. The structures and functions of correlations in neural population codes. *Nature Reviews Neuroscience*, 23:551–567, 2022.

- [16] Allan Pinkus. Approximation theory of the mlp model in neural networks. *Acta numerica*, 8:143–195, 1999.
- [17] Silvere Bonnabel. Stochastic gradient descent on riemannian manifolds. *IEEE Transactions on Automatic Control*, 58(9):2217–2229, 2013.
- [18] Crispin W Gardiner et al. *Handbook of stochastic methods*, volume 3. Springer Berlin, 1985.
- [19] Stephen Coombes. Waves, bumps, and patterns in neural field theories. *Biological cybernetics*, 93:91–108, 2005.
- [20] Wenlian Lu, Enrico Rossoni, and Jianfeng Feng. On a gaussian neuronal field model. *NeuroImage*, 52(3):913–933, 2010.
- [21] Yann LeCun, Léon Bottou, Yoshua Bengio, and Patrick Haffner. Gradient-based learning applied to document recognition. *Proceedings of the IEEE*, 86(11):2278–2324, 1998.
- [22] Matus Telgarsky. Benefits of depth in neural networks. In *Conference on learning theory*, pages 1517–1539. PMLR, 2016.
- [23] Alex Krizhevsky, Geoffrey Hinton, et al. Learning multiple layers of features from tiny images. 2009.
- [24] Yaroslav Bulatov. Notmnist dataset. *Google (Books/OCR), Tech. Rep.[Online]. Available: http://yaroslavvb.blogspot. it/2011/09/notmnist-dataset. html*, 2, 2011.
- [25] Dan Hendrycks and Kevin Gimpel. A baseline for detecting misclassified and out-of-distribution examples in neural networks. In *International Conference on Learning Representations*, 2016.
- [26] Christian Szegedy, Wojciech Zaremba, Ilya Sutskever, Joan Bruna, Dumitru Erhan, Ian Goodfellow, and Rob Fergus. Intriguing properties of neural networks. *arXiv preprint*, 2013.
- [27] Ian J Goodfellow, Jonathon Shlens, and Christian Szegedy. Explaining and harnessing adversarial examples. *stat*, 1050:20, 2015.
- [28] Kexin Pei, Yinzhi Cao, Junfeng Yang, and Suman Jana. Deepxplore: Automated whitebox testing of deep learning systems. In *proceedings of the 26th Symposium on Operating Systems Principles*, pages 1–18, 2017.
- [29] Stuart J Russell. *Artificial intelligence a modern approach*. Pearson Education, Inc., 2010.
- [30] Lingkai Kong, Jimeng Sun, and Chao Zhang. Sde-net: equipping deep neural networks with uncertainty estimates. In *Proceedings of the 37th International Conference on Machine Learning*, pages 5405–5415, 2020.
- [31] Bruno B Averbeck, Peter E Latham, and Alexandre Pouget. Neural correlations, population coding and computation. *Nature Reviews Neuroscience*, 7(5):358–366, 2006.
- [32] James H Schwartz, Thomas M Jessell, and Eric R Kandel. *Principles of neural science*. Elsevier New York, 1991.
- [33] Kyle H Srivastava, Caroline M Holmes, Michiel Vellema, Andrea R Pack, Coen PH Elemans, Ilya Nemenman, and Samuel J Sober. Motor control by precisely timed spike patterns. *Proceedings of the National Academy of Sciences*, 114(5):1171–1176, 2017.
- [34] Ian Goodfellow, Yoshua Bengio, and Aaron Courville. *Deep learning*. MIT press, 2016.
- [35] Ari S Benjamin, Ling-Qi Zhang, Cheng Qiu, Alan A Stocker, and Konrad P Kording. Efficient neural codes naturally emerge through gradient descent learning. *Nature Communications*, 13(1):7972, 2022.
- [36] Artur Luczak, Bruce L McNaughton, and Yoshimasa Kubo. Neurons learn by predicting future activity. *Nature machine intelligence*, 4(1):62–72, 2022.
- [37] Elad Schneidman, Michael J Berry, Ronen Segev, and William Bialek. Weak pairwise correlations imply strongly correlated network states in a neural population. *Nature*, 440(7087):1007–1012, 2006.
- [38] David Dahmen, Hannah Bos, and Moritz Helias. Correlated fluctuations in strongly coupled binary networks beyond equilibrium. *Physical Review X*, 6(3):031024, 2016.
- [39] Edmund T Rolls and Gustavo Deco. *The noisy brain: stochastic dynamics as a principle of brain function*. 2010.
- [40] Matthew Farrell, Stefano Recanatesi, Timothy Moore, Guillaume Lajoie, and Eric Shea-Brown. Gradient-based learning drives robust representations in recurrent neural networks by balancing compression and expansion. *Nature Machine Intelligence*, 4(6):564–573, 2022.
- [41] Emre O Neftci, Hesham Mostafa, and Friedemann Zenke. Surrogate gradient learning in spiking neural networks: Bringing the power of gradient-based optimization to spiking neural networks. *IEEE Signal Processing Magazine*, 36(6):51–63, 2019.
- [42] José Miguel Hernández-Lobato and Ryan Adams. Probabilistic backpropagation for scalable learning of bayesian neural networks. In *International conference on machine learning*, pages 1861–1869. PMLR, 2015.

- [43] Manuel Haußmann, Fred A Hamprecht, and Melih Kandemir. Sampling-free variational inference of bayesian neural networks by variance backpropagation. In *Uncertainty in Artificial Intelligence*, pages 563–573. PMLR, 2020.
- [44] Anqi Wu, Sebastian Nowozin, Edward Meeds, Richard E Turner, Jose Miguel Hernandez-Lobato, and Alexander L Gaunt. Deterministic variational inference for robust bayesian neural networks. *arXiv preprint*, 2018.
- [45] Jannik Schmitt and Stefan Roth. Sampling-free variational inference for neural networks with multiplicative activation noise. In *Pattern Recognition: 43rd DAGM German Conference, DAGM GCPR 2021, Bonn, Germany, September 28–October 1, 2021, Proceedings*, pages 33–47. Springer, 2022.
- [46] Jaime De La Rocha, Brent Doiron, Eric Shea-Brown, Krešimir Josić, and Alex Reyes. Correlation between neural spike trains increases with firing rate. *Nature*, 448(7155):802–806, 2007.
- [47] Jure Zbontar, Li Jing, Ishan Misra, Yann LeCun, and Stéphane Deny. Barlow twins: Self-supervised learning via redundancy reduction. In *International Conference on Machine Learning*, pages 12310–12320. PMLR, 2021.
- [48] Daniel J Amit and MV Tsodyks. Quantitative study of attractor neural network retrieving at low spike rates. I. substrate-spikes, rates and neuronal gain. *Network: Computation in Neural Systems*, 2(3):259, 1991.
- [49] Daniel J Amit and Nicolas Brunel. Dynamics of a recurrent network of spiking neurons before and following learning. *Network: Computation in Neural Systems*, 8(4):373–404, 1997.
- [50] Jacob Steinhardt and Percy S Liang. Unsupervised risk estimation using only conditional independence structure. *Advances in Neural Information Processing Systems*, 29, 2016.
- [51] Diederik P Kingma and Jimmy Ba. Adam: A method for stochastic optimization. *arXiv preprint*, 2014.
- [52] Karen Simonyan and Andrew Zisserman. Very deep convolutional networks for large-scale image recognition. *arXiv preprint*, 2014.
- [53] Max Welling and Yee W Teh. Bayesian learning via stochastic gradient langevin dynamics. In *Proceedings of the 28th international conference on machine learning (ICML-11)*, pages 681–688, 2011.
- [54] Nicolas Boumal. *An introduction to optimization on smooth manifolds*. Cambridge University Press, 2023.
- [55] Halsey Lawrence Royden and Patrick Fitzpatrick. *Real analysis*, volume 32. Macmillan New York, 1988.
- [56] Jianfeng Feng, Yingchun Deng, and Enrico Rossoni. Dynamics of moment neuronal networks. *Physical Review E*, 73(4):041906, 2006.
- [57] Qi Yang, Zhu Zhichao, Wei Yiming, Cao Lu, Wang Zhigang, Lu Wenlian, and Feng Jianfeng. Toward spike-based stochastic neural computing. *arXiv preprint*, 2023.
- [58] Hengyuan Ma, Yang Qi, Pulin Gong, Wenlian Lu, and Jianfeng Feng. Dynamics of bump attractors in neural circuits with emergent spatial correlations. *arXiv preprint*, 2022.
- [59] Yang Qi. An efficient numerical algorithm for the moment neural activation. *arXiv preprint*, 2022.
- [60] Thang Bui, Daniel Hernández-Lobato, Jose Hernandez-Lobato, Yingzhen Li, and Richard Turner. Deep gaussian processes for regression using approximate expectation propagation. In *International conference on machine learning*, pages 1472–1481. PMLR, 2016.
- [61] Durk P Kingma, Tim Salimans, and Max Welling. Variational dropout and the local reparameterization trick. *Advances in neural information processing systems*, 28, 2015.
- [62] Arthur Asuncion and David Newman. Uci machine learning repository, 2007.
- [63] Han Xiao, Kashif Rasul, and Roland Vollgraf. Fashion-mnist: a novel image dataset for benchmarking machine learning algorithms. *arXiv preprint*, 2017.
- [64] Sergey Ioffe and Christian Szegedy. Batch normalization: Accelerating deep network training by reducing internal covariate shift. In *International conference on machine learning*, pages 448–456. pmlr, 2015.

Supplementary Information

Probabilistic computation with emerging covariance: towards efficient uncertainty quantification

Hengyuan Ma¹, Yang Qi^{1,2,3}, Li Zhang⁴, Wenlian Lu^{1,2}, Jianfeng Feng^{1,2,*}

1 Institute of Science and Technology for Brain-inspired Intelligence, Fudan University, Shanghai 200433, China

2 Key Laboratory of Computational Neuroscience and Brain-Inspired Intelligence (Fudan University), Ministry of Education, China

3 MOE Frontiers Center for Brain Science, Fudan University, Shanghai 200433, China

4 School of Data Science, Fudan University, Shanghai 200433, China

** jffeng@fudan.edu.cn*

Contents

1 Derivation of the moment activations (MAs)	2
A. Diffusion approximation for a non-linear stochastic network	2
B. Linear response approximation for covariance activation	3
C. Moment activations for Ornstein–Uhlenbeck processes	3
2 Theoretical properties of supervised mean and unsupervised covariance (SMUC)	4
A. Heaviside case	4
B. General activation functions	10
3 MNN based on leaky integrate-and-fire model	11
4 Theoretical interpretation for how the stochastic model captures the sensitivity via uncertainty	12
5 Numerical verification	13
A. Covariance activations	13
B. MNNs approximate the stochastic neural network	14
6 Comparison with Bayesian variational inference	14
7 Performance comparison with Bayesian variational inference	16
8 Batch-wise covariance trick	17
9 Supplementary results	18
A. Uncertainty quantification on Heaviside MNNs	18
B. Further comparison of using correlation and not using correlation	19

1 Derivation of the moment activations (MAs)

A. Diffusion approximation for a non-linear stochastic network

In this section, we employ the diffusion approximation [48, 49] to derive the mean and variance activation for a general non-linear stochastic neural network. Consider a non-linear stochastic neural network

$$\frac{dx_i}{dt} = f_i(x_i) + \sum_{j=1}^N w_{ij}v_j + v_{s,i} \quad i = 1, \dots, N, \quad (\text{S1})$$

$$v_i = h_i(x_i), \quad i = 1, \dots, N, \quad (\text{S2})$$

$$v_{s,i} = \mu_{s,i} + \sigma_{s,i}\xi_{s,i}, \quad i = 1, \dots, N, \quad (\text{S3})$$

where x_i is the state of the i -th neuron, $f_i(\cdot)$ is a real-value function which governs the dynamics of x_i , v_i is the signal produced by the i -th neuron, which is transmitted to other neurons through the connection weight w_{ij} , $h_i(\cdot)$ is a real-value signal function of the i -th neuron that maps the state of i -th neuron to its signal v_i , $v_{s,i}$ is the stochasticity of the i -th neuron, which is a Brownian motion with drift $\mu_{s,i}$ and diffusion coefficient $\sigma_{s,i}^2$.

We assume that the system reaches a steady-state distribution, i.e., the distribution of x_i and v_i are independent of time t . In general, this steady-state distribution can not be solved analytically. Nevertheless, if we assume that the number of the neurons N is large, the absolute values of weight connections w_{ij} are small, and the correlations between neurons are weak, we can simplify the system by diffusion approximation [48, 49]. Concretely, we approximate the weighted received signals $\sum_{j=1}^N w_{ij}v_j + v_{s,i}$ by a Brownian motion $\bar{\mu}_i + \bar{\sigma}_i\xi_i$, where the drift $\bar{\mu}_i$ and diffusion coefficient $\bar{\sigma}_i^2$ are determined by the weight matrix $W = (w_{ij})$ and the joint distribution of $(v_{s,i}, v_j, j = 1, \dots, N)$. We further assume that $v_{s,i}$ is independent of $v_i, i = 1, \dots, N$ and $v_{s,i}$ are independent from each other. Denote the mean and covariance of $(v_j, j = 1, \dots, N)$ as

$$\mu_i = \mathbb{E}[v_i], \quad C_{ij} = \mathbb{E}[(v_i - \mu_i)(v_j - \mu_j)]. \quad (\text{S4})$$

For $1 \leq i, j \leq N$, we have

$$\bar{\mu}_i = \sum_{j=1}^N w_{ij}\mu_j + \mu_{s,i}, \quad \bar{\sigma}_i^2 = \sum_{l,k=1}^N w_{il}C_{lk}w_{ik} + \sigma_{s,i}^2. \quad (\text{S5})$$

Additionally, the covariance between $\bar{\mu}_i + \bar{\sigma}_i\xi_i$ and $\bar{\mu}_j + \bar{\sigma}_j\xi_j$ as

$$\bar{C}_{ij} = \sum_{l,k=1}^N w_{il}C_{lk}w_{jk}. \quad (\text{S6})$$

In this way, the equation Eq. (S1) can be rewritten as

$$\frac{dx_i}{dt} = f_i(x_i) + \bar{\mu}_i + \bar{\sigma}_i\xi_i \quad i = 1, \dots, N. \quad (\text{S7})$$

Denote the steady-state distribution of each x_i as $p(x_i|\bar{\mu}_i, \bar{\sigma}_i^2)$ and steady-state distribution of each pair x_i, x_j as $p(x_i, x_j|\bar{\mu}_i, \bar{\mu}_j, \bar{\sigma}_i^2, \bar{\sigma}_j^2, \bar{C}_{ij})$. These distributions can be determined through Fokker-Planck equation [18]. The distribution $p(x_i|\bar{\mu}_i, \bar{\sigma}_i^2)$ is the solution of the partial differential equation (PDE)

$$\frac{\partial}{\partial x_i} ((f_i(x_i) + \bar{\mu}_i)p(x_i)) = \frac{\bar{\sigma}_i^2}{2} \frac{\partial^2}{\partial x_i^2} p(x_i), \quad (\text{S8})$$

and the joint distribution $p(x_i, x_j|\bar{\mu}_i, \bar{\mu}_j, \bar{\sigma}_i^2, \bar{\sigma}_j^2, \bar{C}_{ij})$ is the solution of the PDE

$$\left(\frac{\partial}{\partial x_i} (f_i(x_i) + \bar{\mu}_i) + \frac{\partial}{\partial x_j} (f_j(x_j) + \bar{\mu}_j) \right) p(x_i, x_j) = \left(\frac{\bar{\sigma}_i^2}{2} \frac{\partial^2}{\partial x_i^2} + \frac{\bar{\sigma}_j^2}{2} \frac{\partial^2}{\partial x_j^2} + \bar{C}_{ij} \frac{\partial^2}{\partial x_i \partial x_j} \right) p(x_i, x_j). \quad (\text{S9})$$

After solving the state-steady distributions, we can calculate the first two moments

$$\mathbb{E}[v_i] = \int h_i(x_i)p(x_i|\bar{\mu}_i, \bar{C}_i)dx_i, \quad (\text{S10})$$

$$\mathbb{E}[(v_i - \mu_i)(v_j - \mu_j)] = \int (h_i(x_i) - \mathbb{E}[v_i])(h_j(x_j) - \mathbb{E}[v_j])p(x_i, x_j|\bar{\mu}_i, \bar{\mu}_j, \bar{\sigma}_i^2, \bar{\sigma}_j^2, \bar{C}_{ij})dx_i dx_j. \quad (\text{S11})$$

The above mean field approximation should satisfies the self-consistent conditions, i.e.,

$$\mu_i = \int h_i(x_i) p(x_i | \bar{\mu}_i, \bar{C}_i) dx_i \quad (S12)$$

$$C_{ij} = \int \int (h_i(x_i) - \mathbb{E}[v_i])(h_j(x_j) - \mathbb{E}[v_j]) p(x_i, x_j | \bar{\mu}_i, \bar{\mu}_j, \bar{\sigma}_i^2, \bar{\sigma}_j^2, \bar{C}_{ij}) dx_i dx_j, \quad (S13)$$

and Eq. (S5),(S6),(S8),(S9). We call Eq. (S12)-(S13) as the *mean activation* and *variance activation* respectively.

B. Linear response approximation for covariance activation

In this section, we derive covariance activation based on the linear response theory [46]. Rewrite the dynamics of two neurons i and j in the system Eq. (S1)-(S3) with correlated inputs ($i \neq j$) as

$$\frac{dx_i}{dt} = f_i(x_i) + \bar{\mu}_i + \bar{\sigma}_i \eta_i + \bar{\sigma}_i ((\sqrt{1-c} - 1) \eta_i + \sqrt{c} \eta), \quad (S14)$$

$$\frac{dx_j}{dt} = f_j(x_j) + \bar{\mu}_j + \bar{\sigma}_j \eta_j + \bar{\sigma}_j ((\sqrt{1-c} - 1) \eta_j + \sqrt{c} \eta), \quad (S15)$$

where η_i, η_j and η are independent standard Brownian motions, c is the correlation coefficient of the input signals of two neurons calculated as $c = \bar{C}_{ij}/(\bar{\sigma}_i \bar{\sigma}_j)$, which is assumed to be relatively small ($c \ll 1$) under a weak correlation assumption. Since c is small, we treat the term $\bar{\sigma}_i ((\sqrt{1-c} - 1) \eta_i + \sqrt{c} \eta)$ and $\bar{\sigma}_j ((\sqrt{1-c} - 1) \eta_j + \sqrt{c} \eta)$ are the small perturbation parameterized by c . The covariance between the output signals of two neurons $\mathbb{E}[(v_i - \mu_i)(v_j - \mu_j)]$ can be considered as a function of c , denoted as $C_{v,ij}(c)$. Since c is small, we can approximate $C_{v,ij}(c)$ by first-order Taylor expansion as

$$C_{v,ij}(c) \sim \frac{d}{dc} C_{v,ij}(0) c, \quad (S16)$$

where the derivative $\frac{d}{dc} C_{v,ij}(0)$ can be considered as a sort of susceptibility describing how two neurons transfer weak correlated input signals [46]. The specific form of susceptibility $\frac{d}{dc} C_{v,ij}(0)$ depends on the dynamics of two neurons. We call Eq. (S16) as the *covariance activation*.

C. Moment activations for Ornstein–Uhlenbeck processes

We now develop the MAs for the Ornstein–Uhlenbeck system (Eq. (6)) in the main paper, where the dynamics of each neuron is

$$\frac{dx_i}{dt} = -x_i + \bar{\mu}_i + \sqrt{2} \bar{\sigma}_i \xi_i, \quad v_i = h_i(x_i), \quad i = 1, \dots, N. \quad (S17)$$

This process has the unique steady-state distribution which is a Gaussian distribution

$$p(x_i | \bar{\mu}_i, \bar{\sigma}_i^2) = \mathcal{N}(x_i; \bar{\mu}_i, \bar{\sigma}_i^2) = \frac{1}{\sqrt{2\pi\bar{\sigma}_i^2}} \exp\left\{-\frac{(x_i - \bar{\mu}_i)^2}{2\bar{\sigma}_i^2}\right\} \quad (S18)$$

and the joint distribution of (x_i, x_j)

$$p(x_i, x_j | \bar{\mu}_i, \bar{\mu}_j, \bar{\sigma}_i^2, \bar{\sigma}_j^2, \bar{C}_{ij}) = \mathcal{N}\left((\bar{\mu}_i, \bar{\mu}_j), \begin{pmatrix} \bar{\sigma}_i^2 & -c_{ij} \bar{\sigma}_i \bar{\sigma}_j \\ -c_{ij} \bar{\sigma}_i \bar{\sigma}_j & \bar{\sigma}_j^2 \end{pmatrix}\right) \quad (S19)$$

$$= \frac{1}{2\pi\sqrt{1-c_{ij}^2}\bar{\sigma}_i\bar{\sigma}_j} \exp\left(-\frac{1}{2(1-c_{ij}^2)\bar{\sigma}_i^2\bar{\sigma}_j^2}(x_i - \bar{\mu}_i, x_j - \bar{\mu}_j) \begin{pmatrix} \bar{\sigma}_i^2 & -c_{ij} \bar{\sigma}_i \bar{\sigma}_j \\ -c_{ij} \bar{\sigma}_i \bar{\sigma}_j & \bar{\sigma}_j^2 \end{pmatrix} (x_i - \bar{\mu}_i, x_j - \bar{\mu}_j)^T\right), \quad (S20)$$

where $c_{ij} = \bar{C}_{ij}/(\bar{\sigma}_i \bar{\sigma}_j)$ is the correlation coefficient between the inputs of the i -th and j -th neurons. In the following, we denote $\bar{\sigma}_i^2$ as \bar{C}_i for convenience. Using Eq. (S10)-(S11), we can write out the mean and variance of the output signals v_i at the steady-state distribution

$$m_{v,i}(\bar{\mu}_i, \bar{C}_i) := \mathbb{E}[v_i] = \int h_i(x_i) p(x_i | \bar{\mu}_i, \bar{C}_i) dx_i, \quad (S21)$$

$$C_{v,i}(\bar{\mu}_i, \bar{C}_i) := \mathbb{E}[(v_i - \mathbb{E}[v_i])^2] = \int h_i^2(x_i) p(x_i | \bar{\mu}_i, \bar{C}_i) dx_i - m_{v,i}(\bar{\mu}_i, \bar{C}_i)^2, \quad (S22)$$

Using Eq. (S16), the approximated covariance is

$$C_{v,ij}(\bar{\mu}_i, \bar{\mu}_j, \bar{C}_i, \bar{C}_j, \bar{C}_{ij}) \approx \frac{1}{2\pi} \int h_i(\sigma_i x_i + \mu_i) \exp(-\frac{1}{2}x_i^2) x_i dx_i \int h_j(\sigma_j x_j + \mu_j) \exp(-\frac{1}{2}x_j^2) x_j dx_j c_{ij}, \quad (\text{S23})$$

which can be rewritten as

$$C_{v,ij}(\bar{\mu}_i, \bar{C}_i, \bar{\mu}_j, \bar{C}_j, c) = \chi_i(\bar{\mu}_i, \bar{C}_i) \chi_j(\bar{\mu}_j, \bar{C}_j) c_{ij}, \quad (\text{S24})$$

where

$$\chi_i(\bar{\mu}_i, \bar{C}_i) = \frac{1}{\sqrt{2\pi}} \int h_i(\sqrt{\bar{C}_i} x + \bar{\mu}_i) e^{-\frac{x^2}{2}} dx. \quad (\text{S25})$$

2 Theoretical properties of supervised mean and unsupervised covariance (SMUC)

Supposed that the output (label) \mathbf{y} of the dataset are generated by a parameterized stochastic network (Eq. (6)) receiving the input \mathbf{x} at its first layer, and we aim to train the MNN through SMUC for learning its parameters $(W^{(l)}, \mathbf{b}^{(l)})$. Noticed that σ_l are hyper-parameters and do not participate in the training. We prove three theoretical results:

- SMUC is equivalent to stochastic Riemannian gradient descent,
- After trained by SMUC, MNNs can produce ground-truth mean and variance at each layer even if σ_l of the stochastic network are unknown, as long as we set them as arbitrary positive values,
- Under mild conditions, as the number of the layers goes to infinity, the output covariance converges to the ground-truth one.

We first consider the situation that all the activations are Heaviside function, and then we generalize the results to other activation functions.

A. Heaviside case

We start from the case where the network has only one non-linear layer. Consider the mapping $\mathbf{x} \mapsto q(\mathbf{y}|\mathbf{x})$ that is described by the stochastic process

$$\begin{aligned} \frac{d\mathbf{x}^{(1)}}{dt} &= -\mathbf{x}^{(1)} + \mathbf{x} + \sqrt{2}C_{\text{in}}^{\frac{1}{2}}\boldsymbol{\xi}^{(1)}, \quad \mathbf{v}^{(1)} = \mathbf{x}^{(1)}, \\ \frac{d\mathbf{x}^{(2)}}{dt} &= -\mathbf{x}^{(2)} + W\mathbf{v}^{(1)} + \mathbf{b} + \sqrt{2}\sigma\boldsymbol{\xi}^{(2)}, \quad \mathbf{v}^{(2)} = \mathbf{h}(\mathbf{x}^{(2)}) \\ \frac{d\mathbf{y}}{dt} &= -\mathbf{y} + \mathbf{v}^{(2)} \end{aligned} \quad (\text{S26})$$

where $\mathbf{x} = (x_i)_{i=1}^m \in \mathbb{R}^m$ is the input and $\mathbf{y} = (y_k)_{k=1}^n \in \mathbb{R}^n$ is the output, \mathbf{h} is the element-wise Heaviside function, $W = (\mathbf{w}_k^T)_{k=1}^n$ with $\mathbf{w}_k^T \in \mathbb{R}^m$ is the ground-truth weights, $\mathbf{b} = (b_k)_{k=1}^n \in \mathbb{R}^n$ are the ground-truth biases, $\boldsymbol{\xi}^{(l)}$ are standard Brownian motions, $\sigma > 0$ is a constant, and $C_{\text{in}} \in \mathbb{R}^{m \times m}$ is the unknown diffusion matrix (positive definite). Note that here the covariance matrix of the noise added to the input \mathbf{x} can be arbitrary positive definite matrix, no need to be supposed as a scalar matrix as that in Eq. (6) in the main paper. In this way, the result derived here can be directly utilized for multiple-layer cases later. Under stationary state, we simplify the above stochastic via diffusion approximation and obtain

$$y_k = h(\mathbf{w}_k^T[\mathbf{x} + C_{\text{in}}^{\frac{1}{2}}\mathbf{z}] + b_k + \sigma u_k), \quad \mathbf{z} \sim \mathcal{N}(\mathbf{0}, I_m), \quad u_k \sim \mathcal{N}(0, 1), \quad k = 1, \dots, n. \quad (\text{S27})$$

For convenience, we introduce an augmented input $\mathbf{x}' = (\mathbf{x}, 1) \in \mathbb{R}^{m+1}$, augmented weights $\mathbf{w}'_k = (\mathbf{w}_k, b_k) \in \mathbb{R}^{m+1}$ which include the bias terms as their component, augmented covariance matrix

$$\begin{pmatrix} C_{\text{in}} & \mathbf{0} \\ \mathbf{0}^T & 0 \end{pmatrix}, \quad (\text{S28})$$

and augmented noise term $\mathbf{z}' = (\mathbf{z}, z)$ with $z \sim \mathcal{N}(0, 1)$ and write

$$y_k = h(\mathbf{w}_k^T[\mathbf{x} + C_{\text{in}}^{\frac{1}{2}}\mathbf{z}] + \sigma u_k), \quad \mathbf{z} \sim \mathcal{N}(\mathbf{0}, I_m), \quad u_k \sim \mathcal{N}(0, 1), \quad k = 1, \dots, n, \quad (\text{S29})$$

where we use the original notations and do not increase the dimension m by 1 for convenient. Using the definition of the moment mapping and Eq. (S29), we have the ground-truth mean and covariance (variance) are

$$\mu_{y,k}(\mathbf{x}) = m_v(\bar{\mu}_k, \bar{C}_k), \quad C_{y,k}(\mathbf{x}) = C_v(\bar{\mu}_k, \bar{C}_k), \quad k = 1, \dots, n, \quad (S30)$$

$$C_{y,kj}(\mathbf{x}) = \chi(\bar{\mu}_k, \bar{C}_k)\chi(\bar{\mu}_j, \bar{C}_j)c_{kj}, \quad k, j = 1, \dots, n, \quad k \neq j, \quad (S31)$$

with

$$\bar{\mu}_k = \mathbf{w}_k^T \mathbf{x}, \quad \bar{C}_{kj} = \mathbf{w}_k^T C_{\text{in}} \mathbf{w}_j + \delta_{kj} \sigma^2, \quad \bar{C}_k = \bar{C}_{kk}, \quad c_{kj} = \frac{\bar{C}_{kj}}{\sqrt{\bar{C}_k \bar{C}_j}}, \quad (S32)$$

where $\delta_{kj} = 1$ if $k = j$ else $\delta_{kj} = 0$. To learn the mapping $\mathbf{x} \mapsto q(\mathbf{y}|\mathbf{x})$ (Eq. (S27)) up to its second moments, we construct a single layer MNN in which the feed-forward propagation for an input \mathbf{x} is calculated as

$$\tilde{m}_{y,k}(\mathbf{x}) = m_v(\tilde{\mu}_k, \tilde{C}_k), \quad \tilde{C}_{y,k}(\mathbf{x}) = C_v(\tilde{\mu}_k, \tilde{C}_k), \quad k = 1, \dots, n, \quad (S33)$$

$$\tilde{C}_{y,kj}(\mathbf{x}) = \chi(\tilde{\mu}_k, \tilde{C}_k)\chi(\tilde{\mu}_j, \tilde{C}_j)\tilde{c}_{kj}, \quad k, j = 1, \dots, n, \quad k \neq j, \quad (S34)$$

with

$$\tilde{\mu}_k = \tilde{\mathbf{w}}_k^T \mathbf{x}, \quad \tilde{C}_{kj} = \tilde{\mathbf{w}}_k^T \tilde{C}_{\text{in}} \tilde{\mathbf{w}}_j + \delta_{kj} \tilde{\sigma}^2, \quad \tilde{C}_k = \tilde{C}_{kk}, \quad \tilde{c}_{kj} = \frac{\tilde{C}_{kj}}{\sqrt{\tilde{C}_k \tilde{C}_j}}, \quad (S35)$$

where \tilde{y} is the predicted y using its mean and $(\tilde{\mathbf{w}}_1, \dots, \tilde{\mathbf{w}}_n)$ are the weights to be learned, \tilde{C}_{in} and $\tilde{\sigma}$ are the manually set, which may be different from C_{in} and σ . Note that in the case of Eq. (5) of the main paper, we set \tilde{C}_{in} as $\sigma_1^2 I$ and σ here corresponds to σ_2 . The choice of \tilde{C}_{in} is arbitrary, as long as it is positive definite. Denote the objective function as loss $\mathcal{L}(\mathbf{y}, \tilde{\mu}_y)$, where $\tilde{\mu}_y = (\tilde{m}_{y,k})_{k=1}^m$. For training we apply the gradient descent

$$\tilde{\mathbf{w}}_{k,t+1} = \tilde{\mathbf{w}}_{k,t} - \gamma_t \frac{\partial \mathcal{L}}{\partial \tilde{\mathbf{w}}_{k,t}}, \quad k = 1, \dots, n, \quad t = 1, \dots, T \quad (S36)$$

as optimizer, where γ_t is the learning rate, and T is the step number of training. Once again, we would like to emphasize that all second moments are treated as constants during gradient calculation and do not participate in back-propagation.

Using the MAs, we can approximate \mathbf{y} by a Gaussian distribution using its first two moments as

$$\mathbf{y} \sim \mu_y + C_y^{\frac{1}{2}} \mathbf{z}, \quad \mathbf{z} \sim \mathcal{N}(\mathbf{0}, I), \quad (S37)$$

where $\mu_y = (\mu_{y,k})_{k=1}^n$, and $C_y = (C_{y,kj})_{k,j=1}^n$. Using this approximation, the objective can be rewritten as

$$\mathcal{L}(\mathbf{y}, \tilde{\mu}_y) \sim \mathcal{L}(\mu_y, \tilde{\mu}_y) + J(\mu_y, \tilde{\mu}_y) C_y^{\frac{1}{2}} \mathbf{z}, \quad (S38)$$

where $J(\mu_y, \tilde{\mu}_y)$ is the Jacobi matrix of the function $\mathcal{L}(\mathbf{y}, \tilde{\mu}_y)$ at $\mathbf{y} = \mu_y$. Then the gradient at the t step can be approximately rewritten as the summation of the deterministic part

$$\frac{\partial}{\partial \tilde{\mathbf{w}}_{k,t}} \mathcal{L}(\mu_y, \tilde{\mu}_y) \quad (S39)$$

with a stochastic term

$$\xi_{k,t} = \frac{\partial \mathcal{L}}{\partial \tilde{\mathbf{w}}_{k,t}} J(\mu_y, \tilde{\mu}_y) C_y^{\frac{1}{2}} \mathbf{z}. \quad (S40)$$

Note that the mean activation of Heaviside function satisfies

$$m_v(\mu, C) = m_v(a\mu, a^2 C), \quad \forall a > 0, \mu \in \mathbb{R}, C > 0. \quad (S41)$$

Denote $\alpha_{k,t} = \sqrt{\frac{\bar{C}_k}{\bar{C}_{k,t}}}$, where $\tilde{C}_{k,t} = \tilde{\mathbf{w}}_{k,t}^T \tilde{C}_{\text{in}} \tilde{\mathbf{w}}_{k,t} + \tilde{\sigma}^2$ then we have

$$\mathcal{L}(\mu_y, \tilde{\mu}_y) = \mathcal{L}((m_v(\bar{\mu}_k, \bar{C}_k))_{k=1}^n, (m_v(\tilde{\mu}_{k,t}, \tilde{C}_{k,t}))_{k=1}^n) \quad (S42)$$

$$= \mathcal{L}((m_v(\bar{\mu}_k, \bar{C}_k))_{k=1}^n, (m_v(\alpha_{k,t} \tilde{\mathbf{w}}_{k,t}^T \mathbf{x}, \alpha_{k,t}^2 \tilde{C}_{k,t}))_{k=1}^n) \quad (S43)$$

$$= \mathcal{L}((m_v(\bar{\mu}_k, \bar{C}_k))_{k=1}^n, (m_v(\hat{\mathbf{w}}_{k,t}^T \mathbf{x}, \bar{C}_k))_{k=1}^n), \quad (S44)$$

where we define $\hat{\mathbf{w}}_{k,t} = \alpha_{k,t} \tilde{\mathbf{w}}_{k,t}$. Hence, we have

$$\frac{\partial}{\partial \tilde{\mathbf{w}}_{k,t}} \mathcal{L}((m_v(\bar{\mu}_k, \bar{C}_k))_{k=1}^n, (m_v(\tilde{\mathbf{w}}_{k,t}^T \mathbf{x}, \bar{C}_k))_{k=1}^n) = \alpha_{k,t} \frac{\partial}{\partial \hat{\mathbf{w}}_{k,t}} \mathcal{L}((m_v(\bar{\mu}_k, \bar{C}_k))_{k=1}^n, (m_v(\hat{\mathbf{w}}_{k,t}^T \mathbf{x}, \bar{C}_k))_{k=1}^n). \quad (\text{S45})$$

As a result, we can write the update equation Eq. (S36) as

$$\tilde{\mathbf{w}}_{k,t+1} = \tilde{\mathbf{w}}_{k,t} - \gamma_t [\alpha_{k,t} \frac{\partial}{\partial \hat{\mathbf{w}}_{k,t}} \mathcal{L}((m_v(\bar{\mu}_k, \bar{C}_k))_{k=1}^n, (m_v(\hat{\mathbf{w}}_{k,t}^T \mathbf{x}, \bar{C}_k))_{k=1}^n) + \boldsymbol{\xi}_{k,t}] \quad (\text{S46})$$

$$\alpha_{k,t} \tilde{\mathbf{w}}_{k,t+1} = \alpha_{k,t} \tilde{\mathbf{w}}_{k,t} - \gamma_t [\alpha_{k,t}^2 \frac{\partial}{\partial \hat{\mathbf{w}}_{k,t}} \mathcal{L}((m_v(\bar{\mu}_k, \bar{C}_k))_{k=1}^n, (m_v(\hat{\mathbf{w}}_{k,t}^T \mathbf{x}, \bar{C}_k))_{k=1}^n) + \alpha_{k,t} \boldsymbol{\xi}_{k,t}] \quad (\text{S47})$$

$$\alpha_{k,t} \tilde{\mathbf{w}}_{k,t+1} = \hat{\mathbf{w}}_{k,t} - \gamma_t [\alpha_{k,t}^2 \frac{\partial}{\partial \hat{\mathbf{w}}_{k,t}} \mathcal{L}((m_v(\bar{\mu}_k, \bar{C}_k))_{k=1}^n, (m_v(\hat{\mathbf{w}}_{k,t}^T \mathbf{x}, \bar{C}_k))_{k=1}^n) + \alpha_{k,t} \boldsymbol{\xi}_{k,t}] \quad (\text{S48})$$

If we track the weights $\hat{\mathbf{w}}_{k,t}$ at each step t , the update of weight in Eq. (S36) is equivalent to two steps

$$\check{\mathbf{w}}_{k,t+1} = \hat{\mathbf{w}}_{k,t} - \gamma_t (\alpha_{k,t}^2 \frac{\partial}{\partial \hat{\mathbf{w}}_{k,t}} \mathcal{L}_{\text{mean}} + \alpha_{k,t} \boldsymbol{\xi}_{k,t}) \quad (\text{S49})$$

$$\hat{\mathbf{w}}_{k,t+1} = \frac{\alpha_{k,t+1}}{\alpha_{k,t}} \check{\mathbf{w}}_{k,t+1}, \quad (\text{S50})$$

where $\mathcal{L}_{\text{mean}}$ is the loss on the first moment taking the second moments as the constants

$$\mathcal{L}_{\text{mean}} = \mathcal{L}((m_v(\bar{\mu}_k, \bar{C}_k))_{k=1}^n, (m_v(\hat{\mathbf{w}}_{k,t}^T \mathbf{x}, \bar{C}_k))_{k=1}^n). \quad (\text{S51})$$

The first step is minimizing $\mathcal{L}_{\text{mean}}$ using Stochastic gradient Langevin dynamics (SGLD) [53]. The second step can be consider a retraction step in *stochastic Riemannian gradient descent* [17]. Specifically, define the manifold $\mathcal{M} = \mathcal{M}_1 \otimes \mathcal{M}_2 \otimes \dots \otimes \mathcal{M}_n \in \mathbb{R}^{m \times n}$, where \otimes is the Cartesian product, and

$$\mathcal{M}_k = \{\hat{\mathbf{w}} \in \mathbb{R}^m, \hat{\mathbf{w}}^T \bar{C}_{\text{in}} \hat{\mathbf{w}} + \alpha_{k,t}^2 \tilde{\sigma}^2 = \bar{C}_k\}, \quad k = 1, \dots, n. \quad (\text{S52})$$

Note that according to the definition of $\alpha_{k,t}^2$, we always have

$$\alpha_{k,t}^2 \tilde{\sigma}^2 < \bar{C}_k, \quad (\text{S53})$$

hence \mathcal{M}_k is not empty. We call \mathcal{M} as iso-variance sphere, as the weights $(\hat{\mathbf{w}}_k)$ assigned by it ensure that the mean activation $m_v(\cdot, \cdot)$ receives the ground-truth variance \bar{C}_k , as described in Eq. (S44). At each iteration, we first update the parameters by gradient descent in the Euclidean space ignoring the manifold constrain (Eq. (S49)), and then we project the parameters back to the manifold \mathcal{M} (Eq. (S50)). Thus, we are actually implementing a *stochastic Riemannian gradient descent* [54] on the iso-variance sphere, and Eq. (S49)-(S50) can be rewritten as

$$\hat{\omega}_{t+1} = R_{\hat{\omega}_t} [-\gamma_t (\alpha_t^2 \odot \frac{\partial}{\partial \hat{\omega}_t} \mathcal{L}_{\text{mean}} + \alpha_t \odot \boldsymbol{\xi}_t)], \quad (\text{S54})$$

where $\hat{\omega}_t \in \mathbb{R}^{m \times n}$ is the concatenation of $(\hat{\mathbf{w}}_{k,t}, k = 1, \dots, n)$, $\boldsymbol{\xi}_t$ is the concatenation of $(\boldsymbol{\xi}_{k,t}, k = 1, \dots, n)$, $R_{\hat{\omega}}$ is a retraction on \mathcal{M} [54], α_t is the concatenation of $(\alpha_{k,t}, k = 1, \dots, n)$, and \odot is the block-wise multiplication defined as

$$\alpha_t^2 \odot \frac{\partial}{\partial \hat{\omega}_t} \mathcal{L}_{\text{mean}} = (\alpha_{k,t}^2 \frac{\partial}{\partial \hat{\mathbf{w}}_{k,t}} \mathcal{L}_{\text{mean}}, k = 1, \dots, n), \quad \alpha_t \odot \boldsymbol{\xi}_t = (\alpha_{k,t} \boldsymbol{\xi}_{k,t}, k = 1, \dots, n). \quad (\text{S55})$$

The retraction $R_{\hat{\omega}}$ is a first-order approximation of the corresponding exponential map $\exp_{\hat{\omega}}$ on \mathcal{M} [54], which induces the following gradient descent iteration

$$\hat{\omega}_{t+1} = \exp_{\hat{\omega}_t} [-\gamma_t (\alpha_t^2 \odot \frac{\partial}{\partial \hat{\omega}_t} \mathcal{L}_{\text{mean}} + \alpha_t \odot \boldsymbol{\xi}_t)]. \quad (\text{S56})$$

The convergence of Eq. (S56) has been investigated in [17]. Denote

$$H(\hat{\omega}_t, \boldsymbol{\xi}_t) = \frac{\partial}{\partial \hat{\omega}_t} \mathcal{L}_{\text{mean}} + \boldsymbol{\xi}_t \oslash \alpha_t, \quad (\text{S57})$$

where \oslash is the block-wise division defined as

$$\boldsymbol{\xi}_t \oslash \alpha_t = (\frac{\boldsymbol{\xi}_{k,t}}{\alpha_{k,t}}, k = 1, \dots, n). \quad (\text{S58})$$

According to Thm.3 of [17], for the stochastic Riemannian gradient descent iteration, if the following conditions are satisfied:

(1) the learning rate γ_t and $\alpha_{k,t}$ satisfy the standard condition

$$\sum_t \gamma_t^2 \alpha_{k,t}^4 < +\infty, \quad \sum_t \gamma_t \alpha_{k,t}^2 = +\infty, \quad \forall k = 1, \dots, n, \quad (\text{S59})$$

(2) there exists a compact set $K \subset \mathbb{R}^m$, such that

$$\hat{\omega}_t \in K, \quad \forall t > 0, \quad (\text{S60})$$

(3) \mathcal{M} is a Hadamard manifold, and satisfies

(3a) there is a point $\nu \in \mathcal{M}$ and $S > 0$, such that

$$\inf_{\omega: D(\omega, \nu) > S} \langle \exp_{\omega}^{-1}(\nu), \frac{\partial}{\partial \omega} \mathcal{L}_{\text{mean}} \rangle < 0, \quad (\text{S61})$$

where $D(\omega, \nu)$ is the squared geodesic distance of ω and ν on \mathcal{M} ,

(3b) there exists a lower bound on the sectional curvature denoted by $\kappa < 0$,

(3c) there exists a continuous function $f : \mathcal{M} \rightarrow \mathbb{R}$ that satisfies

$$\begin{aligned} f(\omega)^2 &\geq \max\{1, \mathbb{E}_{\xi}[\|H(\omega, \xi)\|^2 (1 + \sqrt{|\kappa|}(\sqrt{D(\omega, \nu)} + \|H(\omega, \xi)\|))], \\ &\quad \mathbb{E}_{\xi}[(2\|H(\omega, \xi)\| \sqrt{D(\omega, \nu)} + \|H(\omega, \xi)\|^2)^2]\} \end{aligned} \quad (\text{S62})$$

then the iterations

$$\hat{\omega}_{t+1} = \exp_{\hat{\omega}_t} \left[-\frac{\gamma_t}{f(\hat{\omega}_t)} (\alpha_t^2 \odot \frac{\partial}{\partial \hat{\omega}_t} \mathcal{L}_{\text{mean}} + \alpha_t \odot \xi_t) \right]. \quad (\text{S63})$$

converges to the point where the gradient $\frac{\partial}{\partial \hat{\omega}_t} \mathcal{L}_{\text{mean}}$ vanishes almost sure, i.e.,

$$\frac{\partial}{\partial \hat{\omega}_t} \mathcal{L}_{\text{mean}} \rightarrow 0, \text{ a.s.} \quad (\text{S64})$$

The condition (2) is satisfied, since \mathcal{M} is bounded. The condition (3a) and (3b) are satisfied, since \mathcal{M} is the product of spheres \mathcal{M}_k embedded in the Euclidean space. The condition (3c) is satisfied, since \mathcal{M} is bounded and $\xi_{k,t}$ are Gaussian. Hence the condition (1) is the only one to be determined. Accordingly, if we select the proper steps $\{\gamma_t\}$, the gradient will converge to zero almost surely.

Supposed that $\hat{\mathbf{w}}_k = \mathbf{w}_k$ is the only solution that vanishes the gradient. Then, after convergence, the trained weight $\tilde{\mathbf{w}}_k$ satisfies

$$\tilde{m}_{y,k}(\mathbf{x}) = m_v(\tilde{\mathbf{w}}_k^T \mathbf{x}, \tilde{\mathbf{w}}_k^T \tilde{C}_{\text{in}} \tilde{\mathbf{w}}_k + \tilde{\sigma}^2) = m_v(\alpha_k \mathbf{w}_k^T \mathbf{x}, \mathbf{w}_k^T C_{\text{in}} \mathbf{w}_k + \sigma^2) = m_v(\bar{\mu}_k, \bar{C}_k) = \mu_{y,k}, \quad (\text{S65})$$

where $\alpha_k = \sqrt{\frac{\bar{C}_k}{C_k}}$. Therefore, the trained MNN can fit the ground-truth mean output. For the variance activation of the Heaviside function (Eq. (11)), we also have

$$C_v(\mu, C) = C_v(a\mu, a^2 C), \quad \forall a > 0, \mu \in \mathbb{R}, C > 0 \quad (\text{S66})$$

hence

$$\tilde{C}_{y,k}(\mathbf{x}) = C_{y,k} \quad (\text{S67})$$

Therefore, the trained MNN can also fit the ground-truth variance output *without knowing C_{in} and σ* . Additionally, when $\tilde{\mathbf{w}}_{k,t}^T \tilde{C}_{\text{in}} \tilde{\mathbf{w}}_{k,t} > \bar{C}_k$, the step-size $\alpha_{t,k} \gamma_t$ is reduced; when $\tilde{\mathbf{w}}_{k,t}^T \tilde{C}_{\text{in}} \tilde{\mathbf{w}}_{k,t} < \bar{C}_k$, the step-size $\alpha_{t,k} \gamma_t$ is amplified. $\alpha_{k,t}$ can be considered as a regularizer: when the model underestimates the variance ($\tilde{\mathbf{w}}_{k,t}^T \tilde{C}_{\text{in}} \tilde{\mathbf{w}}_{k,t} > \bar{C}_k$), $\alpha_{k,t}$ slows down the gradient descent; when the model overestimate the variance ($\tilde{\mathbf{w}}_{k,t}^T \tilde{C}_{\text{in}} \tilde{\mathbf{w}}_{k,t} < \bar{C}_k$), $\alpha_{k,t}$ accelerates the gradient descent.

Next, we analyze the output covariance of the model. Similar, according to Eq. (12), we also have

$$\chi(\mu, C) = \chi(a\mu, a^2 C), \quad \forall a > 0, \mu \in \mathbb{R}, C > 0 \quad (\text{S68})$$

and hence

$$\chi(\tilde{\mathbf{w}}_k^T \mathbf{x}, \bar{C}_k) = \chi(\bar{\mu}_k, \bar{C}_k) \quad (\text{S69})$$

However, we have

$$\tilde{C}_{y,kj}(\mathbf{x}) = \chi(\tilde{\mathbf{w}}_k^T \mathbf{x}, \tilde{C}_k) \chi(\tilde{\mathbf{w}}_j^T \mathbf{x}, \tilde{C}_j) \frac{\tilde{\mathbf{w}}_k^T \tilde{C}_{\text{in}} \tilde{\mathbf{w}}_j}{\sqrt{\tilde{C}_k \tilde{C}_j}} \quad (\text{S70})$$

$$= \chi(\bar{\mu}_k, \bar{C}_k) \chi(\bar{\mu}_j, \bar{C}_j) \frac{\alpha_k \alpha_j \tilde{\mathbf{w}}_k^T \tilde{C}_{\text{in}} \tilde{\mathbf{w}}_j}{\sqrt{(\alpha_k^2 \bar{C}_k)(\alpha_j^2 \bar{C}_j)}} \quad (\text{S71})$$

$$= \chi(\bar{\mu}_k, \bar{C}_k) \chi(\bar{\mu}_j, \bar{C}_j) \frac{\mathbf{w}_k^T \tilde{C}_{\text{in}} \mathbf{w}_j}{\sqrt{C_k C_j}}, \quad k, j = 1, \dots, n, \quad k \neq j. \quad (\text{S72})$$

It is observed that unless $\mathbf{w}_k^T \tilde{C}_{\text{in}} \mathbf{w}_j = \mathbf{w}_k^T C_{\text{in}} \mathbf{w}_j$, we cannot ensure that the output covariance is as the same as the ground-truth one $C_{y,kj}$. For scalar output ($n = 1$), this is not an issue. For multi-dimensional cases, however, it seems that we need to know the ground-truth input covariance C_{in} for the learning the ground-truth covariance of output.

Nevertheless, we show that under some mild conditions, when the number of the layers goes to infinity, we can also learn the ground-truth covariance of output without knowing C_{in} . First, we notice that the above results can be easily generalized to multi-layer cases. Concretely, the following L -layer network

$$\begin{aligned} \frac{d\mathbf{x}^{(1)}}{dt} &= -\mathbf{x}^{(1)} + \mathbf{x} + \sqrt{2} C_{\text{in}}^{\frac{1}{2}} \boldsymbol{\xi}^{(1)}, \quad \mathbf{v}^{(1)} = \mathbf{x}^{(1)}, \\ \frac{d\mathbf{x}^{(l)}}{dt} &= -\mathbf{x}^{(l-1)} + W^{(l-1)} \mathbf{v}^{(l-1)} + \mathbf{b} + \sqrt{2} \sigma_l \boldsymbol{\xi}^{(l)}, \quad \mathbf{v}^{(l)} = \mathbf{h}(\mathbf{x}^{(l)}), \quad l = 2, \dots, L \\ \frac{d\mathbf{y}}{dt} &= -\mathbf{y} + W^{(L)} \mathbf{v}^{(L)}. \end{aligned} \quad (\text{S73})$$

where $W^{(l)} \in \mathbb{R}^{m^{(l+1)} \times m^{(l)}}$ are weight matrices, $\mathbf{b}^{(l)}$ are bias terms, $\boldsymbol{\xi}^{(l)}$ are standard Brownian motions, $\sigma_l > 0$ are constants, and \mathbf{h} is the element-wise Heaviside function. Under stationary state, we simplify the above stochastic via diffusion approximation and obtain

$$\begin{aligned} \mathbf{v}^{(1)} &= \mathbf{x} + C_{\text{in}}^{\frac{1}{2}} \mathbf{z}_{\text{in}} \\ \mathbf{v}^{(l)} &= \mathbf{h}(W^{(l-1)} \mathbf{v}^{(l-1)} + \mathbf{b}^{(l-1)} + \sigma_l \mathbf{z}^{(l)}), \quad \mathbf{z}^{(l)} \sim \mathcal{N}(\mathbf{0}, I_{n^{(l)}}), \quad l = 2, \dots, L \\ \mathbf{y} &= W^{(L)} \mathbf{v}^{(L)}, \end{aligned} \quad (\text{S74})$$

Here we can also absorb all the bias terms and noise terms by introducing augment inputs, augmented weights, augmented covariance matrices and augmented noises as we did in Sec. 2, and write

$$\begin{aligned} \mathbf{v}^{(1)} &= \mathbf{x} + C_{\text{in}}^{\frac{1}{2}} \mathbf{z}_{\text{in}} \\ \mathbf{v}^{(l)} &= \mathbf{h}(W^{(l-1)} \mathbf{v}^{(l-1)} + \sigma_l \mathbf{z}^{(l)}), \quad l = 2, \dots, L \\ \mathbf{y} &= W^{(L)} \mathbf{v}^{(L)}. \end{aligned} \quad (\text{S75})$$

Denote $C^{(l)}$ as the covariance of $\mathbf{v}^{(l)}$, $(\tilde{W}^{(l)})_{l=0}^{L-1}$ as the weight matrices of the network to be trained. According to the chain rule, for each layer l , $i = 1, \dots, n^{(l+1)}$, $j = 1, \dots, n^{(l)}$, we have

$$\frac{\partial \mathcal{L}}{\partial \tilde{W}_{ij}} = \frac{\partial \mathcal{L}}{\partial v_i^{(l+1)}} \frac{\partial v_i^{(l+1)}}{\partial \tilde{W}_{ij}}. \quad (\text{S76})$$

Hence, we can replace \mathbf{x} in Eq. (S29) by $\mathbf{v}^{(l)}$, replace C_{in} in Eq. (S75) by $C^{(l)}$ and replace \tilde{C}_{in} in Eq. (S29) by $\tilde{C}^{(l)}$, then the remain analysis is as the same for each layer l . Therefore, after trained, the MNN learns the ground-truth weight matrices, means and variances for each layer. Denote

$$\chi(W_{i\bullet}^{(l)} \mathbf{v}^{(l)}, W_{i\bullet}^{(l)} C^{(l)} (W_{i\bullet}^{(l)})^T + \sigma_l^2) = \chi_i^{(l)}, \quad (\text{S77})$$

where $W_{i\bullet}^{(l)}$ is the row vector $(W_{ij}^{(l)})_{j=1}^{n^{(l)}}$. According to Eq. (S69), we have $\tilde{\chi}_i^{(l)} = \chi_i^{(l)}$. Then according to Eq. (S72), for $i \neq j$, we have

$$\left| C_{ij}^{(l+1)} - \tilde{C}_{ij}^{(l+1)} \right| = \left| \frac{\chi_i^{(l)} \chi_j^{(l)}}{\sqrt{(W_{i\bullet}^{(l)} C^{(l)} (W_{i\bullet}^{(l)})^\top + \sigma_l^2) (W_{j\bullet}^{(l)} C^{(l)} (W_{j\bullet}^{(l)})^\top + \sigma_l^2)}} \sum_{k,q} W_{ik}^{(l)} W_{jq}^{(l)} (C_{kq}^{(l)} - \tilde{C}_{kq}^{(l)}) \right| \quad (\text{S78})$$

$$\leq \left| \chi_i^{(l)} \chi_j^{(l)} \right| \frac{\sum_{k,q} \left| W_{ik}^{(l)} \right| \left| W_{jq}^{(l)} \right|}{\sqrt{(W_{i\bullet}^{(l)} C^{(l)} (W_{i\bullet}^{(l)})^\top + \sigma_l^2) (W_{j\bullet}^{(l)} C^{(l)} (W_{j\bullet}^{(l)})^\top + \sigma_l^2)}} \max_{k,q} \left| C_{kq}^{(l)} - \tilde{C}_{kq}^{(l)} \right| \quad (\text{S79})$$

$$\leq \left| \chi_i^{(l)} \chi_j^{(l)} \right| \frac{n^{(l)} \left\| W_{i\bullet}^{(l)} \right\|_2 \left\| W_{j\bullet}^{(l)} \right\|_2}{\sqrt{(\lambda_{\min}(C^{(l)}) \left\| W_{i\bullet}^{(l)} \right\|_2^2 + \sigma_l^2) (\lambda_{\min}(C^{(l)}) \left\| W_{j\bullet}^{(l)} \right\|_2^2 + \sigma_l^2)}} \max_{k,q} \left| C_{kq}^{(l)} - \tilde{C}_{kq}^{(l)} \right| \quad (\text{S80})$$

$$= \left| \chi_i^{(l)} \chi_j^{(l)} \right| \frac{n^{(l)} \max_{k,q} \left| C_{kq}^{(l)} - \tilde{C}_{kq}^{(l)} \right|}{\sqrt{\lambda_{\min}(C^{(l)})^2 + \lambda_{\min}(C^{(l)}) \sigma_l^2 \left(\frac{\left\| W_{i\bullet}^{(l)} \right\|_2^2}{\left\| W_{j\bullet}^{(l)} \right\|_2^2} + \frac{\left\| W_{j\bullet}^{(l)} \right\|_2^2}{\left\| W_{i\bullet}^{(l)} \right\|_2^2} \right) + \sigma_l^4 \frac{1}{\left\| W_{i\bullet}^{(l)} \right\|_2^2 \left\| W_{j\bullet}^{(l)} \right\|_2^2}}} \quad (\text{S81})$$

$$\leq \left| \chi_i^{(l)} \chi_j^{(l)} \right| \frac{n^{(l)}}{\sqrt{\lambda_{\min}(C^{(l)})^2 + 2\lambda_{\min}(C^{(l)}) \sigma_l^2}} \max_{k,q} \left| C_{kq}^{(l)} - \tilde{C}_{kq}^{(l)} \right|, \quad (\text{S82})$$

where $\|\cdot\|_2$ is the l_2 norm of vectors, and $\lambda_{\min}(C^{(l)})$ is the minimal eigenvalue of $C^{(l)}$. Denote the infinity norm of a vector or matrix as $\|\cdot\|_\infty$. In the above, we have use the Cauchy-Schwarz inequality

$$\sum_{k,q} \left| W_{ik}^{(l)} \right| \left| W_{jq}^{(l)} \right| = (\sum_k \left| W_{ik}^{(l)} \right|) (\sum_k \left| W_{jk}^{(l)} \right|) \leq \sqrt{n^{(l)}} \left\| W_{i\bullet}^{(l)} \right\|_2 \sqrt{n^{(l)}} \left\| W_{j\bullet}^{(l)} \right\|_2 = n^{(l)} \left\| W_{i\bullet}^{(l)} \right\|_2 \left\| W_{j\bullet}^{(l)} \right\|_2, \quad (\text{S83})$$

and the the arithmetic mean inequality

$$\frac{\left\| W_{i\bullet}^{(l)} \right\|_2^2 + \left\| W_{j\bullet}^{(l)} \right\|_2^2}{\left\| W_{j\bullet}^{(l)} \right\|_2^2 + \left\| W_{i\bullet}^{(l)} \right\|_2^2} \geq 2 \sqrt{\frac{\left\| W_{i\bullet}^{(l)} \right\|_2^2 \left\| W_{j\bullet}^{(l)} \right\|_2^2}{\left\| W_{j\bullet}^{(l)} \right\|_2^2 \left\| W_{i\bullet}^{(l)} \right\|_2^2}} = 2 \quad (\text{S84})$$

Then we have

$$\left\| C^{(l+1)} - \tilde{C}^{(l+1)} \right\|_\infty \leq \frac{n^{(l)} \chi_i^{(l)} \chi_j^{(l)}}{\sqrt{\lambda_{\min}(C^{(l)})^2 + 2\lambda_{\min}(C^{(l)}) \sigma_l^2}} \left\| C^{(l)} - \tilde{C}^{(l)} \right\|_\infty, \quad (\text{S85})$$

since $\chi_i^{(l)} > 0$ (see Eq. (12)). Define the *covariance error rate* at the l -layer $r^{(l)}$ as

$$r^{(l)} = \frac{n^{(l)} \chi_i^{(l)} \chi_j^{(l)}}{\sqrt{\lambda_{\min}(C^{(l)})^2 + 2(\lambda_{\min}(C^{(l)}) \sigma_l^2)}}, \quad (\text{S86})$$

which describes how the error on the covariance reduces after propagating through the l -layer. Then we have a sufficient condition to guarantee that after infinity layers, the output covariance is exact the real one: The series $-\sum_q \log r_q$ diverges to positive infinity. This is because if so, we have

$$\lim_{l \rightarrow +\infty} \left\| C_{ij}^{(l)} - \tilde{C}_{ij}^{(l)} \right\|_\infty \leq \lim_{l \rightarrow +\infty} \exp(\sum_{q=1}^l \log r_q) \left\| C_{ij}^{(1)} - \tilde{C}_{ij}^{(1)} \right\|_\infty = 0. \quad (\text{S87})$$

In particular, if there exists a $\varsigma \in (0, 1)$ such that

$$r^{(l)} < 1 - \varsigma, \quad \forall l \in \mathbb{Z}_+, \quad (\text{S88})$$

the sufficient condition is satisfied. Based on Eq.(12) and Eq.(S85), in order to reduce the error in the output covariance, it is beneficial to have larger values for $\frac{\mu^{(l)}}{\sqrt{C^{(l)}}}$ and $\lambda_{\min}(C^{(l)})$ and have smaller values for $n^{(l)}$. Note that $\frac{\mu^{(l)}}{\sqrt{C^{(l)}}}$ is the signal-to-noise ratio (SNR) at the l -th layer, which reflects the quality of the inputs from the previous layer, it suggests that a high SNR helps to the decreasing error of covariance. Additionally, the amount $\lambda_{\min}(C^{(l)})$ is related to the fluctuation of the output covariance at the layer l . Accordingly, high output fluctuation may also benefits to the decreasing error of covariance when keeping $\frac{\mu^{(l)}}{\sqrt{C^{(l)}}}$ as the same. Due to the exponential term in the function χ , the covariance rate $r^{(l)}$ exhibits an exponential decrease as the signal-to-noise ratio (SNR) increases. On the other hand, the covariance rate increases linearly with the dimension $n^{(l)}$. Consequently, even in scenarios where the dimension $n^{(l)}$ is high, it is not necessary for the SNR to be excessively large in order to control the error rate effectively.

B. General activation functions

The results in the previous section require the scaling property of the MAs of (Eq. (S41)), which may not be satisfied for general activation function $g(\cdot)$, such as ReLU function. Nevertheless, we can generalize the above results for general activation function via *the simple function approximation theorem* [55], which argues that we can approximate any measurable g by a sequence of linear combination of a sequence of shifted Heaviside functions i.e., $g_n(x) \rightarrow g(x)$ point-wisely as n goes to infinity, where

$$g_n(x) = \sum_{r=1}^{R_n} a_{r_n} h(x - b_{r_n}), \quad n \in \mathbb{N} \quad (\text{S89})$$

satisfying

$$|g_n(x)| \leq |g(x)|, \quad \forall x \in \mathbb{R}, n \in \mathbb{N} \quad (\text{S90})$$

and a_{r_n} and b_{r_n} are constants. This theorem implies that linear combination of the Heaviside functions with different biases b_r can replace any measurable activation function g . To demonstrate the validity of this approximation in training MNNS, particularly in terms of model's output and calculating the derivative of the mean activation with respect to the input mean, we need to establish that

$$\lim_{n \rightarrow +\infty} \int g_n(x) \mathcal{N}(x; \mu, \sigma^2) dx = \int g(x) \mathcal{N}(x; \mu, \sigma^2) dx, \quad \forall \mu, \sigma, \quad (\text{zero-order approximation}), \quad (\text{S91})$$

$$\lim_{n \rightarrow +\infty} \frac{d}{d\mu} \int g_n(x) \mathcal{N}(x; \mu, \sigma^2) dx = \frac{d}{d\mu} \int g(x) \mathcal{N}(x; \mu, \sigma^2) dx, \quad \forall \mu, \sigma, \quad (\text{first-order approximation}), \quad (\text{S92})$$

where we use $\mathcal{N}(x; \mu, \sigma^2)$ to represent the probabilistic density function of a Gaussian distribution with mean μ and variance σ^2 . We prove the above claims for the cases where the activation function g satisfies the following conditions: there exists a positive m , since that

$$\sup_{x \in \mathbb{R}} \frac{|g(x)|}{|x|^m + 1} < +\infty, \quad (\text{S93})$$

which is a mild condition, satisfied by most of common activation functions such as ReLU, tanh, sigmoid. The proof is as follows. For a given μ and σ , given a $\epsilon > 0$, we show that there exists $N(\epsilon)$, such that $\forall n > N(\epsilon)$, we have

$$\left| \lim_{n \rightarrow +\infty} \int g_n(x) \mathcal{N}(x; \mu, \sigma^2) dx - \int g(x) \mathcal{N}(x; \mu, \sigma^2) dx \right| < \epsilon. \quad (\text{S94})$$

Using Eq. (S90), and the condition Eq. (S93), there exists a constant A (independent of n) such that

$$\frac{|g_n(x) - g(x)|}{|x|^m + 1} \leq \frac{|g(x)| + |g_n(x)|}{|x|^m + 1} \leq \frac{2|g(x)|}{|x|^m + 1} \leq A. \quad (\text{S95})$$

Since $(|x|^m + 1)\mathcal{N}(x; \mu, \sigma^2)$ is integrable, we can find a constant $B > 0$, such that

$$A \int_{x \notin [-B, B]} (|x|^m + 1) \mathcal{N}(x; \mu, \sigma^2) dx < \frac{\epsilon}{2}. \quad (\text{S96})$$

Since $[-B, B]$ is a bounded set, we can require g_n uniformly converges to g on $[-B, B]$ [55]. Hence, there exists a $N(\epsilon)$ such that

$$\sup_{x \in [-B, B]} |g_n(x) - g(x)| < \frac{\epsilon}{2}. \quad (\text{S97})$$

Therefore, $\forall n > N(\epsilon)$, we have

$$\left| \int g_n(x) \mathcal{N}(x; \mu, \sigma^2) dx - \int g(x) \mathcal{N}(x; \mu, \sigma^2) dx \right| \quad (\text{S98})$$

$$\leq \int |g_n(x) - g(x)| \mathcal{N}(x; \mu, \sigma^2) dx \quad (\text{S99})$$

$$= \int_{x \in [-B, B]} |g_n(x) - g(x)| \mathcal{N}(x; \mu, \sigma^2) dx + \int_{x \notin [-B, B]} \frac{|g_n(x) - g(x)|}{|x|^m + 1} (|x|^m + 1) \mathcal{N}(x; \mu, \sigma^2) dx \quad (\text{S100})$$

$$< \frac{\epsilon}{2} \int_{x \in [-B, B]} \mathcal{N}(x; \mu, \sigma^2) dx + A \int_{x \notin [-B, B]} (|x|^m + 1) \mathcal{N}(x; \mu, \sigma^2) dx \quad (\text{S101})$$

$$< \frac{\epsilon}{2} + \frac{\epsilon}{2} = \epsilon \quad (\text{S102})$$

The proof of the first-order approximation (Eq. (S92)) is as the same, except replacing $\mathcal{N}(x; \mu, \sigma^2)$ by $\frac{d}{d\mu} \mathcal{N}(x; \mu, \sigma^2)$ in above procedure. It is obvious that we can prove the approximation up to any finite order. Therefore, we can approximate an MNN that utilizes any measurable functions as activation functions with an MNN that employs the Heaviside function as the activation function. This approximation remains valid not only for the model's output but also for the training procedure of the MNN. In doing so, the previous theoretical results of SMUC still apply.

In contrast to MNNs, the aforementioned results do not hold true for approximating a rate-based network using the Heaviside function as activation functions. This is because the derivative of the linear combination of any finite number of Heaviside functions is zero almost everywhere, while the derivative of the activation function g is generally non-zero at various points. In MNNs, the moments of the activation function are smoothed by the Gaussian kernel. Therefore, if we approximate the activation function up to the zeroth order, we can approximate its moments up to any desired order.

3 MNN based on leaky integrate-and-fire model

In [56, 20], the authors analyzed the stochastic dynamics of a spiking neuronal network (SNN) by a set of non-linear mapping describing how the neurons transfer the input spike signals from other neurons. Concretely, the authors studied a network of N neurons with the dynamics of each neuron applying the leaky integrate-and-fire (LIF) model

$$\frac{dV_i}{dt} = -LV_i + \sum_{j=1}^N w_{ij} S_j, \quad i = 1, \dots, N, \quad (\text{S103})$$

where V_i is the membrane potential of the i -th neuron, L is the leaky conductance, w_{ij} is the synaptic weight from neuron j to neuron i , and S_j is the spike train from pre-synaptic neurons. When V_i reaches the firing threshold V_{th} the neuron will release a spike which is transmitted to other connected neurons, and then V_i is reset to the resting potential V_{res} and enters a refractory period T_{ref} . The corresponding moment activations, which we refer to as *LIF moment activations (LIF MAs)*, are as follows [20]

$$m_v(\bar{\mu}, \bar{C}) = \left(T_{\text{ref}} + \frac{2}{L} \int_{I_{\text{lb}}}^{I_{\text{ub}}} g(x) dx \right)^{-1}, \quad (\text{S104})$$

$$C_v(\bar{\mu}, \bar{C}) = \frac{8}{L^2} m_v(\bar{\mu}, \bar{C})^3 \int_{I_{\text{lb}}}^{I_{\text{ub}}} h(x) dx, \quad (\text{S105})$$

$$\chi(\bar{\mu}, \bar{C}) = \frac{\partial}{\partial \bar{\mu}} m_v(\bar{\mu}, \bar{C}) \quad (\text{S106})$$

where T_{ref} is the refractory period with integration bounds $I_{\text{ub}}(\bar{\mu}, \bar{C}) = \frac{V_{\text{th}}L - \bar{\mu}}{\sqrt{LC}}$ and $I_{\text{lb}}(\bar{\mu}, \bar{C}) = \frac{V_{\text{res}}L - \bar{\mu}}{\sqrt{LC}}$. The constant L , V_{res} , and V_{th} are identical to those in Eq. (S103). The pair of Dawson-like functions $g(x)$ and $h(x)$ appearing in Eq. (S104) and Eq. (S105) are

$$g(x) = e^{x^2} \int_{-\infty}^x e^{-u^2} du, \quad h(x) = e^{x^2} \int_{-\infty}^x e^{-u^2} [g(u)]^2 du. \quad (\text{S107})$$

It is important to highlight that in the LIF MAs (Eq. (S104)-(S106)), the mean is the average number of the spike in a unit time interval, the variance is the variance of the number of the spike in a unit time interval, and the covariance between two neuron i and j is the multiplication of their variances and the coherence of their spike train [46].

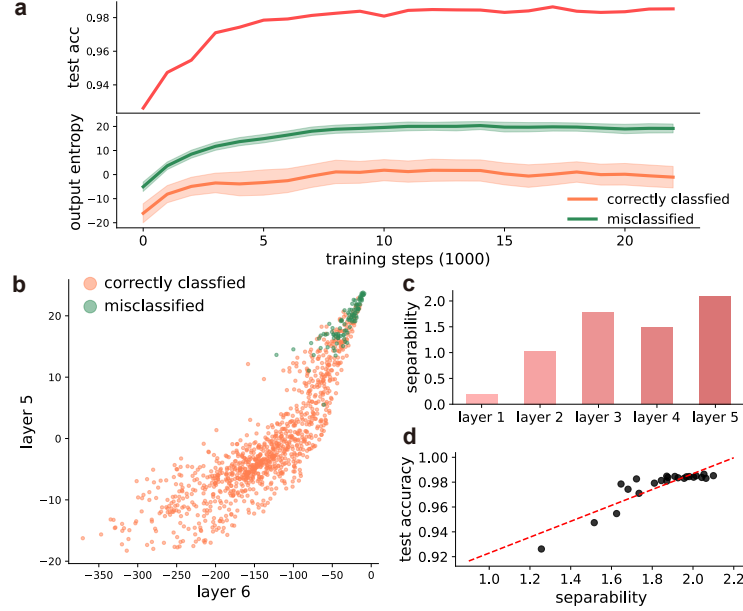


Figure S1: Emerging covariance of LIF MNN faithfully captures the prediction uncertainty. LIF MNN trained on MNIST for image classification. **a**, The training of MNNs on MNIST, with the accuracy (red line) and entropy (orange and green for correctly classified inputs and misclassified inputs respectively) on the test set. The shadows indicate the level of half standard deviations. As the training progresses, the entropy of correctly classified inputs and misclassified inputs diverges. **b**, The entropy of correctly classified and misclassified inputs in the last two layers of MNIST. The misclassified inputs result in relatively higher entropy in both layers. **c**, The entropy separability of correctly classified and misclassified inputs on MNIST increases as the layer index increases. **d**, The relationship between the separability and test accuracy during training on MNIST was analyzed using linear regression. The red dashed line represents the regression line, with coefficients of determination of 0.7760.

Using the LIF MAs, we can construct the corresponding MNN (called *LIF MNN*) with learnable weight connection. After learning, the MNN can be reverted into the corresponding SNN [57], similar as the ReLU and Heaviside MNNs. Compared to the ReLU and Heaviside MNNs, the LIF MNN exhibits more complex MAs, which can pose challenges in its implementation for large-scale models. However, the LIF MNN has well-defined biological plausibility, making it a valuable tool for analyzing the neural circuit mechanisms underlying brain coding and learning processes [58].

As an extension of our study in the main paper, we investigate if the emerging covariance of the LIF MNN can also show high uncertainty on the misclassified samples, compared to the correctly classified samples, after being trained by SMUC. As shown in Fig. S1, we observe the consistent result as that for ReLU (Fig. 2) and Heaviside MNN (Fig. S6).

The implementation is as follows. We set neuron parameters to be $V_{\text{th}} = 20$ mV, $V_{\text{res}} = 0$ mV, $T_{\text{ref}} = 5$ ms, and $\tau = 1/L = 20$ ms, following [20], and conduct the LIF MAs by the efficient numerical algorithm developed in [59]. We construct a fully-connected LIF MNN on MNIST dataset for classification, where the dimension at each layer are 784, 392, 96 and 10, and we add a batch-normalization layer before each non-linearity, following [57]. We apply Adam [51] as the optimizer. The training batch-size is 128, and epoch is 15, the learning rate is 0.0005, and the factor of weight decay is 0.0001.

4 Theoretical interpretation for how the stochastic model captures the sensitivity via uncertainty

As an illustration, we analyze a simple binary logistic regression problem to demonstrate how a stochastic model captures sensitivity through prediction uncertainty. Consider that a binary classification problem, in which $\mathbf{x} \in \mathbb{R}^d$ belongs to the class A if and only if $\mathbf{w}^T \mathbf{x} + b < 0$, otherwise it belongs the class B, where $\mathbf{w} \in \mathbb{R}^d$ and $b \in \mathbb{R}$ are ground-truth parameters. We construct a stochastic logistic regression model

$$y = \Phi(\mathbf{w}^T(\mathbf{x} + \mathbf{z}) + b), \quad \mathbf{z} \sim \mathcal{N}(\mathbf{0}, C), \quad (\text{S108})$$

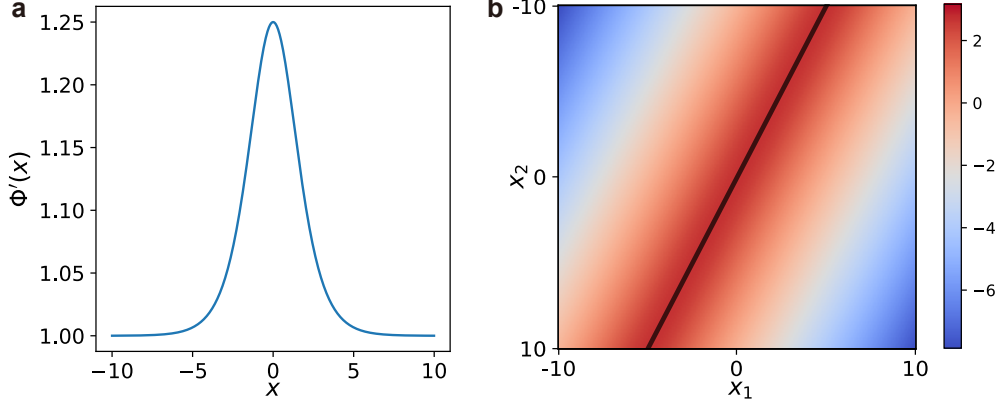


Figure S2: **Stochastic model captures the sensitivity through the prediction uncertainty.** **a**, The derivation of the sigmoid function reaches its maximum at 0. **b**, We demonstrate a two-dimensional instantiation of Eq. (S108). Here we set $\mathbf{w} = (1, 0.5)$, $b = 0$, $C = I$. We calculate the prediction entropy at each $\mathbf{x} \in \mathbb{R}^2$. The closer a point to the decision boundary (black line), the higher the prediction entropy (colored pixels).

where

$$\Phi(s) = \frac{1}{1 + \exp(-s)} \quad (\text{S109})$$

is the sigmoid function, $C \in \mathbb{R}^{d \times d}$ is the covariance matrix of the noise vector \mathbf{z} . The prediction y is stochastic, and the prediction uncertainty is measured by the entropy of its prediction distribution. There is no analytical form of the prediction distribution. Nevertheless, we can calculate it through a linear approximation

$$y = \Phi(\mathbf{w}^T(\mathbf{x} + \mathbf{z}) + b) \approx \Phi(\mathbf{w}^T \mathbf{x} + b) + \Phi'(\mathbf{w}^T \mathbf{x} + b) \mathbf{w}^T \mathbf{z}, \quad (\text{S110})$$

where $\Phi'(s)$ is the derivative of $\Phi(s)$. Hence we can approximate

$$p(y|\mathbf{x}) \approx \mathcal{N}(\Phi(\mathbf{w}^T \mathbf{x} + b), (\Phi'(\mathbf{w}^T \mathbf{x} + b))^2 \mathbf{w}^T C \mathbf{w}), \quad (\text{S111})$$

and its entropy is calculated as

$$H(p(y|\mathbf{x})) \approx \frac{1}{2} (1 + \log 2\pi + \log[(\Phi'(\mathbf{w}^T \mathbf{x} + b))^2 \mathbf{w}^T C \mathbf{w}]). \quad (\text{S112})$$

When \mathbf{x} varies, the entropy $H(p(y|\mathbf{x}))$ also changes. Noticed that $d(\mathbf{x}) = \frac{\mathbf{w}^T \mathbf{x} + b}{\|\mathbf{w}\|}$ is the distance from \mathbf{x} to the decision boundary $\mathbf{w}^T \mathbf{x} + b = 0$. The approximated entropy can be rewritten as

$$H(p(y|\mathbf{x})) \approx \frac{1}{2} (1 + \log 2\pi + \log[(\Phi'(\|\mathbf{w}\| d(\mathbf{x}))^2 \mathbf{w}^T C \mathbf{w})]). \quad (\text{S113})$$

Additionally, noticed that

$$\Phi'(s) = \frac{1}{1 + \exp(-s)} - \frac{1}{(1 + \exp(-s))^2}, \quad (\text{S114})$$

which reaches its maximum at $s = 0$, and monotonically decreases as s goes far away from 0 (Fig. S2a). Therefore, the prediction entropy is higher when \mathbf{x} closer to the decision boundary (Fig. S2b). The closer the \mathbf{x} to the decision boundary, it is easy to push \mathbf{x} to a different class via small perturbation. As a result, we find that the uncertainty (entropy) of the stochastic model indicates the sensitivity.

5 Numerical verification

A. Covariance activations

We numerically verify the accuracy of the covariance activations (Eq. (S25)) for ReLU and Heaviside functions. As illustrated in Fig. S3, we present the signals produced by two neurons $C_{v,ij}$ calculated using the covariance activation, and compare it with the covariance obtained through Monte Carlo simulation. The consistency between these results validate our approach.

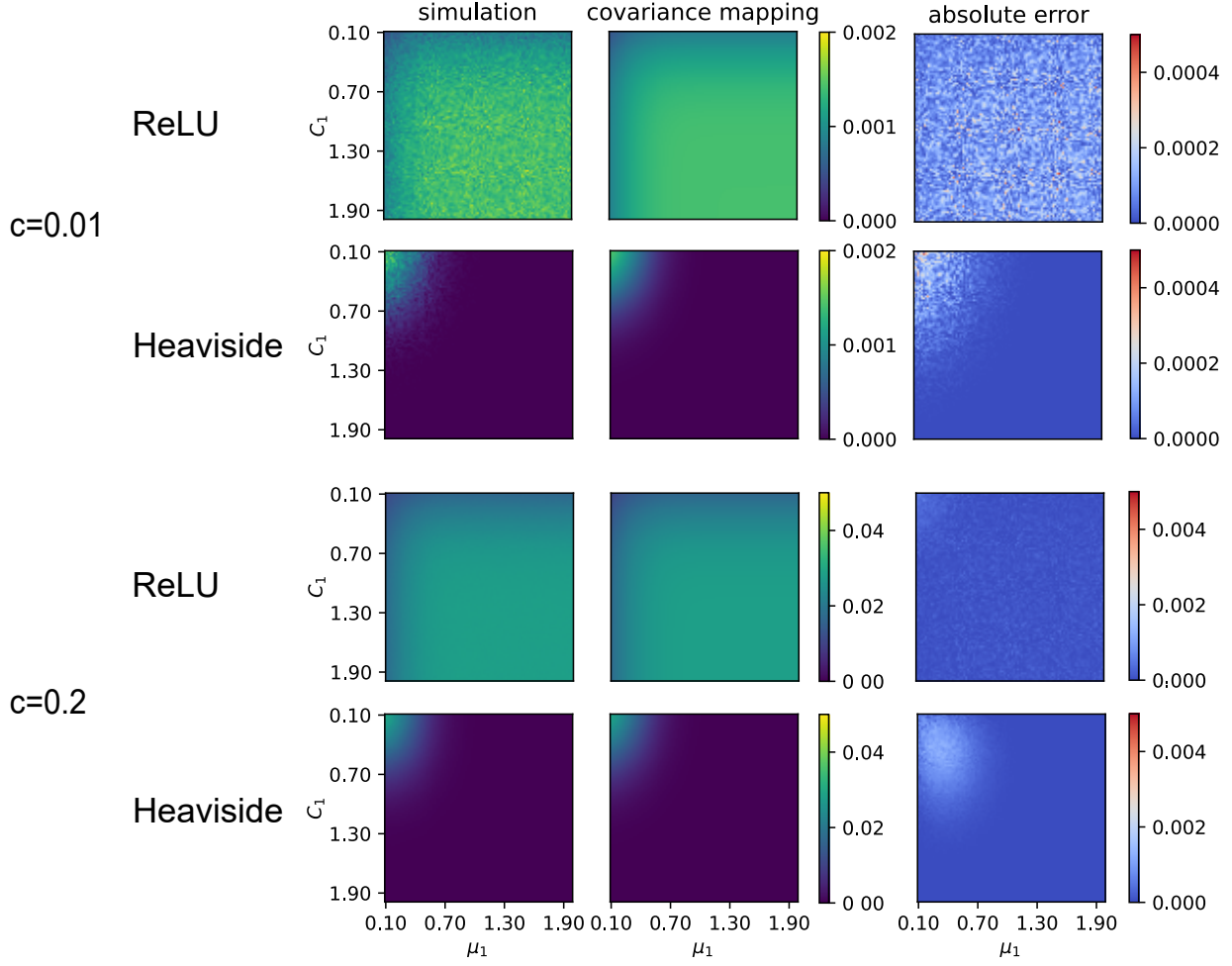


Figure S3: **Numerical verification for covariance activations.** The covariance of the signals produced by two neurons calculated using the covariance activations is consistent with that of Monte Carlo simulations. We present the results with two different correlation levels: a small correlation value of $c = 0.01$ (top) and a relatively larger correlation value of $c = 0.2$ (bottom).

B. MNNs approximate the stochastic neural network

We numerically verify that MNNs can approximate the prediction mean and covariance of the corresponding stochastic neural network. We first train a full-connected ReLU MNN on MNIST for classification, where the dimension of each layer is 784, 196, 48, 10, and set $\sigma_l = 0.2$. The training batch-size is 128, and epoch is 50, the learning rate is 0.0005, and the factor of weight decay is 0.0001. Then we use the trained parameters to construct the corresponding stochastic neural network (Eq. (6)). When provided with an input (Fig. S4a), the stochastic network generates corresponding dynamic patterns. (Fig. S4b). We estimate the output mean, variance and covariance of the stochastic network, and compared it with the that calculated by the MNN (Fig. S4c,d). It is observed that MNN approximates the stochastic network well in terms of the output mean and covariance. We conduct the same experiment for Heaviside MNN, as shown in Fig. S5, and obtain consistent results.

6 Comparison with Bayesian variational inference

We conducted a comparison between our framework and Bayesian variational inference (BVI). To enable a direct comparison, we rewrite the MNN using the steady-state of the stochastic network (Eq. (6)) under the diffusion

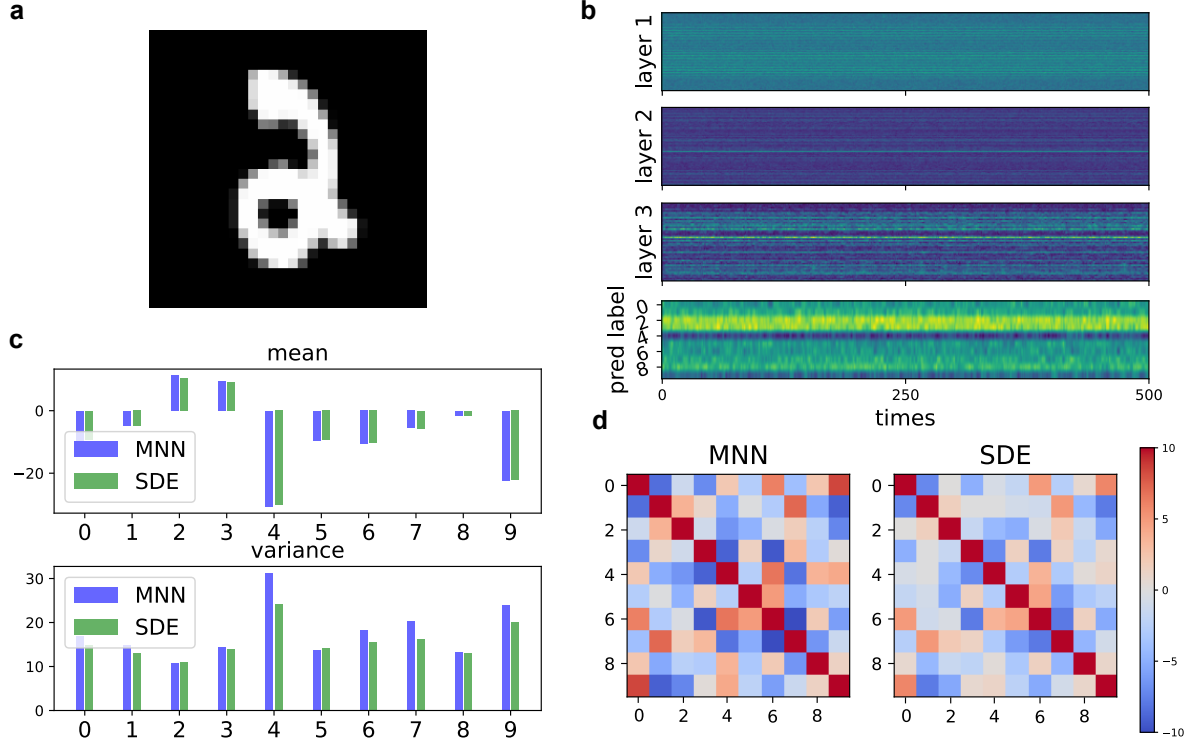


Figure S4: **The ReLU MNN (Eq. (5)) approximates the corresponding stochastic network (Eq. (6)) up to its first two moments.** **a**, The input data from MNIST. **b**, We train an MNN on MNIST and use the parameters of the trained MNN to construct the corresponding stochastic network, and show its dynamics. **c**, The mean and variance produced by MNN and estimated using Monte Carlo methods from the stochastic network. The MNN approximates both mean and variance well, with lower error on the mean. **d**, The covariance matrix produced by MNN and estimated using Monte Carlo methods from the stochastic network. The MNN can approximate the covariance of stochastic network well.

approximation (middle of Fig. 1b)

$$\begin{aligned} \mathbf{v}^{(1)} &= \mathbf{x} + \sigma^{(1)} \mathbf{z}^{(1)} \\ \mathbf{v}^{(l)} &= \mathbf{h}(W^{(l-1)} \mathbf{v}^{(l-1)} + \mathbf{b}^{(l-1)} + \sigma_l \mathbf{z}^{(l)}), \quad l = 2, \dots, L \\ \mathbf{y} &= W^{(L)} \mathbf{v}^{(L)}, \end{aligned} \quad (\text{S115})$$

where \mathbf{z}_l are independent standard Gaussian vectors. After combining the bias $\mathbf{b}^{(l)}$ and the Gaussian vectors $\sigma_l \mathbf{z}^{(l)}$ at each layer, we can regard the biases as stochastic parameters, obeying $\mathcal{N}(\mathbf{b}^{(l)}, \sigma_l^2 I)$. Hence, we can consider the network is parameterized by stochastic parameters θ , and the distribution of θ is parameterized by the trainable parameters ψ , denoted as $q_\psi(\theta)$. Then the variational loss is

$$\mathcal{L}(\theta) = - \int q_\psi(\theta) \log p(\mathbf{y}|\mathbf{x}, \theta) d\theta + \text{KL}(q_\psi(\theta)||p(\theta)), \quad (\text{S116})$$

where $p(\theta)$ is the prior distribution of θ . The right of Eq. (S116) are log-likelihood term and KL-divergence term respectively. We approximate the prediction probability $\int p(\mathbf{y}|\mathbf{x}, \theta) q_\psi(\theta) d\theta$ up to its second moments by a Gaussian distribution $\mathcal{N}(\mu(\mathbf{x}, \psi), C(\mathbf{x}, \psi))$, where the mean and covariance are functions of \mathbf{x} and ψ . Suppose that the loss of the task is mean square error, then the log-likelihood term of variational inference is

$$\mathbb{E}_{\eta \sim \mathcal{N}(\mu(\mathbf{x}, \psi), C(\mathbf{x}, \psi))} [\|\eta - \mathbf{y}\|^2] = \|\mu(\mathbf{x}, \psi) - \mathbf{y}\|^2 + \text{Tr}(C(\mathbf{x}, \psi)). \quad (\text{S117})$$

In our framework, however, only the mean is supervised for minimizing $\|\mu(\mathbf{x}, \psi) - \mathbf{y}\|^2$, and the covariance spontaneously emerges via the non-linear coupling with the mean. Thus, we call BVI as supervised mean and supervised covariance (SMSC), as it supervises both mean and covariance.

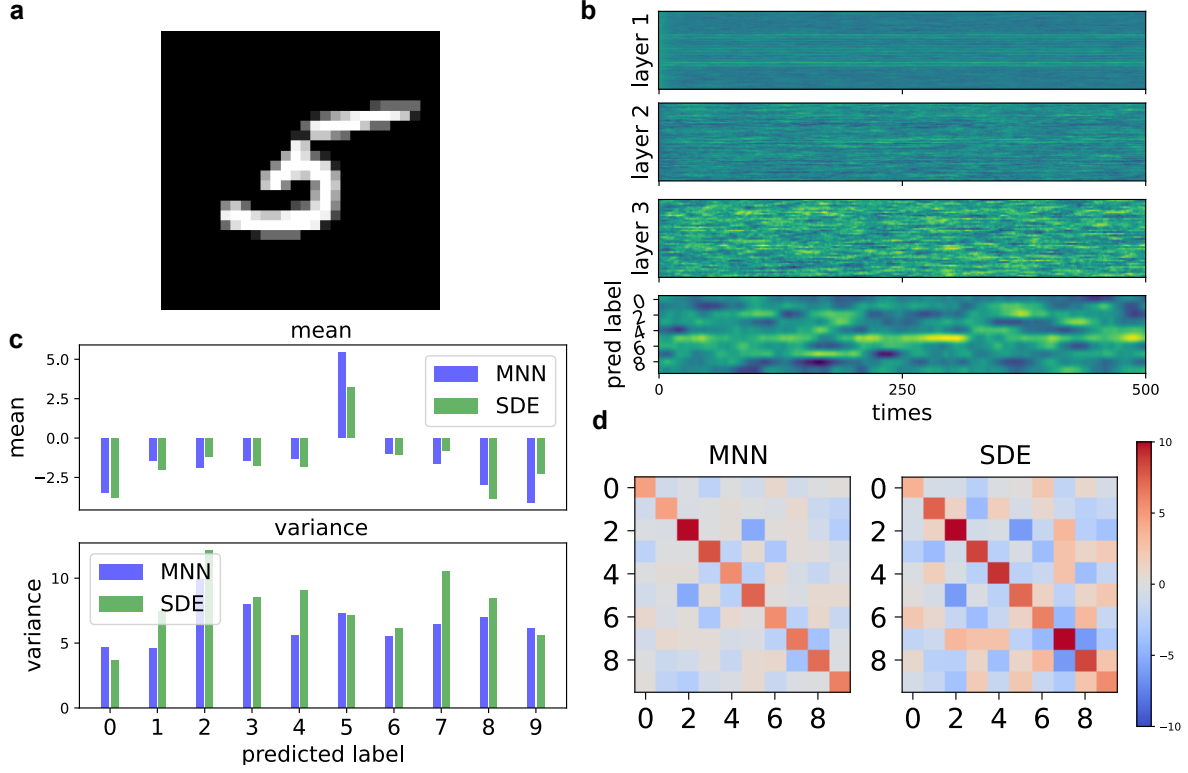


Figure S5: The Heaviside MNN (Eq. (5)) approximates the corresponding stochastic network (Eq. (6)) up to its first two moments. **a**, The input data from MNIST. **b**, We train an MNN on MNIST and use the parameters of the trained MNN to construct the corresponding stochastic network, and show its dynamics. **c**, The mean and variance output by MNN and estimated using Monte Carlo methods from the stochastic network. The MNN approximates both mean and variance well, with lower error on the mean. **d**, The covariance matrix produced by MNN and estimated using Monte Carlo methods from the stochastic network. The MNN can approximate the covariance of stochastic network well.

7 Performance comparison with Bayesian variational inference

We show that our MNNs can achieve comparable or even superior results than representative BVI in terms of model performance. For regression tasks, we train MNNs on UCI regression datasets [62]. We apply min-max renormalization for all the datasets and train our MNNs through SMUC for reducing the mean square error (MSE) loss on the predicted values and ground-truth values. Note that, the MSE loss does not involve prediction covariance. We apply stochastic gradient descent as the optimizer and set the factor of weight decay as zero. The MNN is full-connected and has one hidden layer of width 50, which is the same as that in [45], and set $\sigma_1, \sigma_2 = 0.5, 0.1$. We consider MNN using different activations (ReLU and Heaviside function). To investigate the effect of correlations, we construct dMNN, in which we ignore all the correlations between neurons at each layer. We use *log-likelihood* (LL) on the test set as the metrics, which is calculated as

$$\text{LL}(\mathbf{y}, \boldsymbol{\mu}_y, C_y) = -\frac{1}{2} \left(\log 2\pi C_y + \frac{(\mathbf{y} - \boldsymbol{\mu}_y)^2}{C_y} \right), \quad (\text{S118})$$

where \mathbf{y} is the ground-truth output, $\boldsymbol{\mu}_y, C_y$ are prediction and prediction variance. The log-likelihood (LL) takes into account both the accuracy (mean) and the level of uncertainty (variance). As shown in Table. S1, we compare the log-likelihood of various methods with our MNN, dMNN and show that both MNN and dMNN outperform other methods in most datasets. Additionally, MNN is superior to dMNN for both ReLU and Heaviside functions in most cases, implying that correlation is meaningful. For classification tasks, we train MNNs through SMUC on MNIST, FashionMNIST [63], CIFAR-10 and CIFAR-100 [23] respectively. We use modified LeNet5 as the architecture of MNNs, following the settings in [43]. The training loss is the cross entropy, calculated by the prediction mean and the ground-truth label. As shown in Table. S2, MNNs can achieve comparable performance than other probabilistic computation methods.

Table S1: **Regression results.** Comparison of the average log-likelihood (LL) on the UCI regression datasets over random train/test splits. We implement 20 runs to estimate the standard deviation (in brackets). dMNN means we remove all the covariance during both training and inference. (R) means ReLU activation, (H) represents Heaviside activation. We compare our results with SGLM [53], probabilistic backpropagation (PBP) [42], deep Gaussian process (DGP) [60], multiplicative noise variational inference (MIVI) [45], deterministic variational inference (DVI) [44], Monte Carlo (MC) dropout [10], deep ensembles [13]. The data are results of other methods are from [42, 13, 44, 45]. We bold the highest LL for each dataset.

	boston	concrete	kin8	energy	power	protein	wine	yacht
SGLM	-2.38 (0.06)	-3.01 (0.03)	1.68 (0.00)	-2.21 (0.01)	-2.61 (0.01)	-1.23 (0.01)	0.14 (0.02)	-3.23 (0.03)
PBP	-2.57 (0.09)	-3.16 (0.02)	0.90 (0.01)	-2.04 (0.02)	-2.84 (0.01)	-2.97 (0.00)	-0.97 (0.01)	-1.63 (0.02)
DGP	-2.09 (0.06)	-2.43 (0.02)	2.31 (0.00)	-0.90 (0.01)	-2.39 (0.02)	-1.51 (0.09)	0.37 (0.02)	-0.96 (0.06)
MIVI	-2.43 (0.02)	-3.05 (0.01)	1.15 (0.01)	-1.33 (0.05)	-2.66 (0.01)	-2.99 (0.01)	-0.96 (0.01)	-0.37 (0.02)
DVI	-2.41 (0.02)	-3.06 (0.02)	1.13 (0.00)	-1.01 (0.06)	-2.80 (0.00)	-2.85 (0.01)	-0.90 (0.02)	-0.47 (0.03)
Ensemble	-2.41 (0.25)	-3.06 (0.18)	1.20 (0.02)	-1.38 (0.22)	-2.79 (0.00)	-2.83 (0.02)	-0.94 (0.12)	-1.18 (0.21)
MC Dropout	-2.46 (0.25)	-3.04 (0.09)	0.95 (0.03)	-1.99 (0.09)	-2.89 (0.01)	-2.80 (0.05)	-0.93 (0.05)	-1.55 (0.12)
MNN (R)	0.18 (0.03)	0.17 (0.01)	0.33 (0.00)	0.23 (0.01)	0.07 (0.01)	-0.08 (0.00)	0.36 (0.00)	0.16 (0.02)
dMNN (R)	0.04 (0.01)	0.04 (0.00)	0.06 (0.00)	0.07 (0.00)	0.02 (0.00)	-0.09 (0.00)	0.13 (0.00)	0.04 (0.01)
MNN (H)	0.13 (0.01)	0.09 (0.00)	0.18 (0.00)	0.09 (0.00)	-0.15 (0.00)	-0.05 (0.00)	0.18 (0.00)	0.10 (0.01)
dMNN (H)	-0.25 (0.00)	-0.25 (0.00)	0.00 (0.00)	-0.32 (0.00)	-0.45 (0.00)	-0.34 (0.00)	-0.23 (0.00)	-0.27 (0.00)

Table S2: **Classification results.** Comparison of test accuracy on image classification. We implement 5 runs to estimate the standard deviation (in brackets). We compare MNNs (using ReLU or Heaviside activations, with or without correlations) with three representative uncertainty quantification methods including Dropout (VarOut) [61], deterministic variational inference (DVI) [44], and Variance Back-Propagation (VBP) [43]. The data of other methods are from [43].

	MNN (R)	dMNN (R)	MNN (H)	dMNN (H)	VarOut	DVI	VBP
MNIST	99.04 (0.00)	99.03 (0.02)	99.01 (0.00)	99.05 (0.00)	98.88 (0.05)	99.03 (0.06)	99.15 (0.06)
FashionMNIST	89.85 (0.03)	90.05 (0.00)	90.08 (0.00)	89.93 (0.00)	89.19 (0.24)	89.67 (0.07)	89.90 (0.16)
CIFAR-10	71.04 (0.01)	70.57 (0.48)	70.36 (0.01)	69.63 (0.02)	66.60 (1.06)	64.85 (1.13)	68.67 (1.00)
CIFAR-100	35.56 (0.01)	31.01 (0.03)	40.30 (0.00)	40.04 (0.01)	37.15 (1.43)	33.79 (1.14)	39.03 (1.61)

8 Batch-wise covariance trick

We empirically find that the complexity for training MNNs can be further reduced without significantly sacrificing performance. Addressing computational complexity is a common challenge in probabilistic computation algorithms, particularly when dealing with high-dimensional inputs or large datasets [4]. For MNN and other probabilistic computation algorithms that explicitly calculate covariance matrices such as [44], the main overhead of computation is on the calculating and storing the covariance matrices, which arises $O(d^3)$ time complexity and $O(d^2)$ space complexity. In the case of MNNs and other probabilistic computation algorithms that involve explicit calculations of covariance matrices, such as the approach described in [44], the primary computational overhead lies in the calculation and storage of these covariance matrices. This process incurs a time complexity of $O(d^3)$ and a space complexity of $O(d^2)$, where d represents the data dimensionality. When the covariance matrices are involved into back-propagation, the computational complexity becomes even higher. Luckily, we do not back-propagation on the covariance in MNN. Hence the main complexity comes from the feed-forward propagation. Supposed that the batch size during training is N_{batch} , then to compute a covariance matrix of vectors of dimension d for the whole batch, the space and time complexity are $O(N_{\text{batch}}d^2)$ and $O(N_{\text{batch}}d^3)$ respectively. Inspired by Monte Carlo batch normalization [11], which show that the stochasticity of batch normalization [64] can be used for approximated Bayesian inference. To make MNNs more scalable, instead of calculating the covariance matrix for each input in the batch, we calculate a single covariance matrix for each batch. Supposed that there is a batch of input $\{x_1, x_2, \dots, x_{N_{\text{batch}}}\}$, at layer l , the corresponding means are

$\{\mu_1^{(l)}, \mu_2^{(l)}, \dots, \mu_{N_{\text{batch}}}^{(l)}\}$. We calculate the batch average mean

$$\mu^{(l)} = \frac{1}{N_{\text{batch}}} \sum_{k=1}^{N_{\text{batch}}} \mu_k^{(l)}, \quad l = 1, 2, \dots, L \quad (\text{S119})$$

and use it to calculate the covariance matrix, which is shared for the inputs in this batch

$$C^{(l)} = C_v(W^{(l-1)}\mu^{(l-1)}, W^{(l-1)}C^{(l-1)}(W^{(l-1)})^T), \quad l = 2, \dots, L, \quad (\text{S120})$$

where $C^{(1)} = C^{\text{in}}$, which is set as the same for all the input. In this way, the space and time complexity are reduced to $O(d^2)$ and $O(d^3)$ respectively.

We report the performance of MNN using the batch-wise covariance trick (Methods). As shown in Fig. S6 and Fig. S7, the emerging covariance in the ReLU MNNs using the batch-wise covariance trick also faithfully captures the prediction uncertainty, OOD detection, and adversarial attack awareness, similar as MNNs without batch-wise covariance trick (Fig. 2). We also report the performance of MNNs using the batch-wise covariance trick on the regression and classification tasks in Tab. S3 and Tab. S4 respectively, and we observed that the batch-wise covariance trick only causes marginal degradation compared to the MNNs without the batch-wise covariance trick (Tab. S1 and Tab. S2).

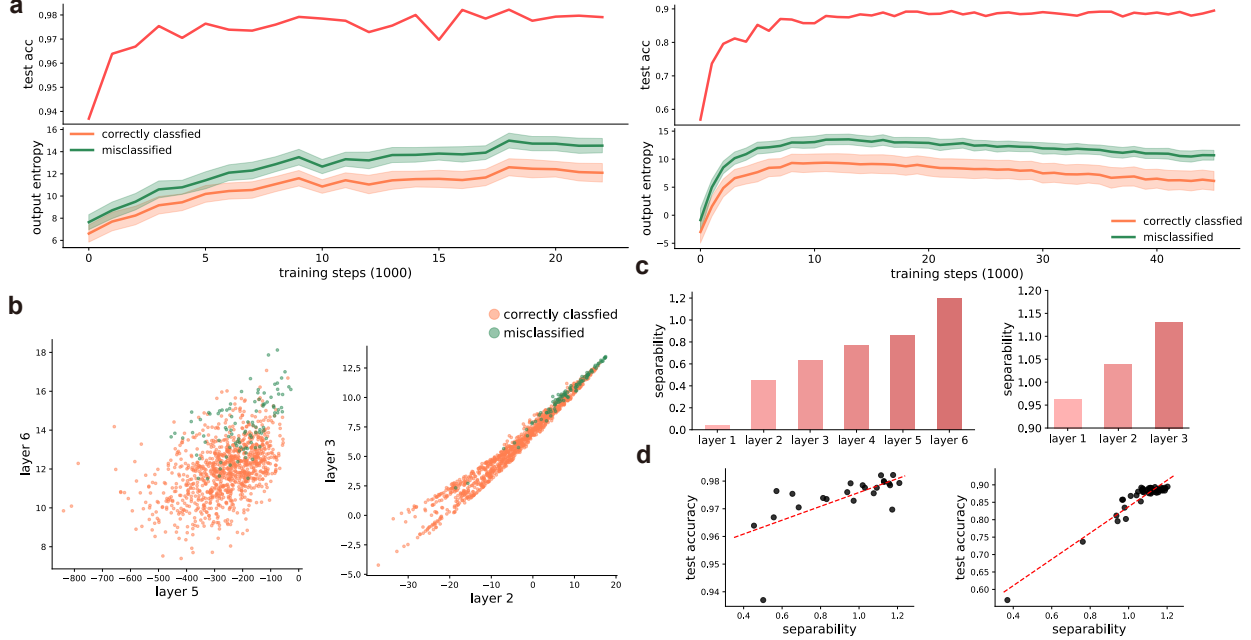


Figure S6: Emerging covariance of MNNs using the batch-wise covariance trick faithfully captures the prediction uncertainty. (Mixed) MNN trained on MNIST (CIFAR-10) for image classification using the batch-wise covariance trick. **a**, The training of MNNs on (left) and CIFAR-10 (right), with the accuracy (red line) and entropy (orange and green for correctly classified inputs and misclassified inputs respectively) on the test set. The shadows indicate the level of half standard deviations. As the training progresses, the entropy of correctly classified inputs and misclassified inputs diverges. **b**, The entropy of correctly classified and misclassified inputs in the last two layers of MNIST (left) and CIFAR-10 (right). The misclassified inputs result in relatively higher entropy in both layers. **c**, The entropy separability of correctly classified and misclassified inputs on MNIST (left) and CIFAR-10 (right) increases as the layer index increases. **d**, The relationship between the separability and test accuracy during training on MNIST (left) and CIFAR-10 (right) was analyzed using linear regression. The red dashed line represents the regression line, with coefficients of determination of 0.4334 for MNIST and 0.8994 for CIFAR-10.

9 Supplementary results

A. Uncertainty quantification on Heaviside MNNs

We report the uncertainty quantification results of Heaviside MNNs for classification in Fig. S8, which is consistent with that of ReLU MNNs in Fig. 2.

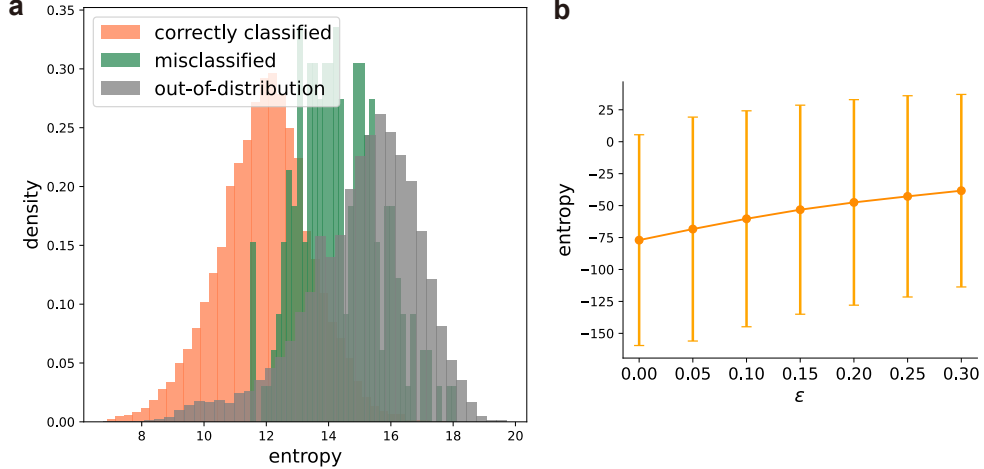


Figure S7: **The emerging covariance of MNN using the batch-wise covariance tricks for out-of-distribution detection and adversarial attack awareness.** **a.** The distribution of entropy on correctly classified, misclassified and out-of-distribution input. **b.** If we do not turn off the variance, although the model is vulnerable to adversarial attack, it can be aware of the attack, reflecting on the increasing of the entropy.

Table S3: **Regression results of MNN using the batch-wise covariance trick.** We report the average log-likelihood (LL) on the UCI regression datasets over random train/test splits. MNN (H) represents Heaviside MNN, and MNN (R) represents ReLU MNN. We implement 20 runs to estimate the standard deviation (in brackets).

	boston	concrete	kin8	energy	power	protein	wine	yacht
MNN (R)	0.12 (0.01)	0.07 (0.01)	0.30 (0.00)	-0.14 (0.01)	-0.56 (0.00)	-0.09 (0.00)	0.16 (0.01)	0.00 (0.02)
MNN (H)	0.13 (0.01)	0.09 (0.00)	0.18 (0.00)	0.09 (0.00)	-0.15 (0.00)	-0.05 (0.00)	0.18 (0.00)	0.10 (0.01)

B. Further comparison of using correlation and not using correlation

We further investigate the impact of disregarding the correlation between neurons on uncertainty quantification. To do so, we repeat the experiments presented in Figure 2 of the main paper, while manually setting all off-diagonal elements of the covariance matrices to zero during the training and inference of MNNs. As shown in Fig. S9a, for MNIST classification (pure MNN), the MNN without correlation has similar performance in terms of test accuracy. However, for CIFAR-10 classification (mixed MNN), MNN without correlation learns much slower compared to the one with correlations, as shown in Fig. S9b. In terms of uncertainty quantification, we compare the separability of the entropy on the correctly classified and misclassified samples across layers for MNIST (Fig. S9c) and CIFAR-10 (Fig. S9d) classification. It is observed that for CIFAR-10, there is only a slight decrease in separability when omitting the correlation between neurons. On the other hand, for MNIST, there is a relatively larger decrease in separability. This difference can be attributed to the fact that in the mixed MNN, the inputs are initially decorrelated by the convolution layers. As a result, the correlations in the layers that utilize MAs become less crucial for uncertainty quantification. However, as demonstrated in Figure S9b, these correlations still play a role in facilitating faster learning.

Table S4: **Classification results.** The test accuracy of MNNs trained using batch-wise covariance trick on image classification.

	MNN (R)	MNN (H)
MNIST	98.99 (0.00)	99.00 (0.00)
FashionMNIST	89.66 (0.00)	90.13 (0.00)
CIFAR-10	70.75 (0.01)	69.86 (0.01)
CIFAR-100	35.84 (0.02)	40.21 (0.02)

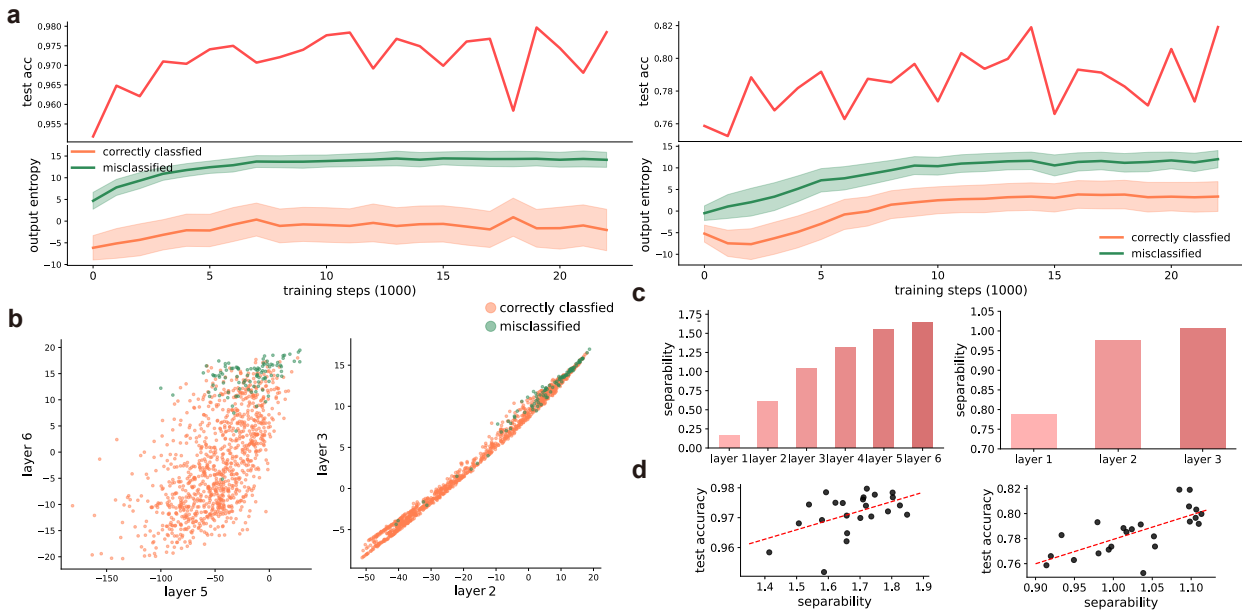


Figure S8: **Emerging covariance of Heaviside MNNs faithfully captures the prediction uncertainty.** (Mixed) Heaviside MNN trained on MNIST (CIFAR-10) for image classification. **a**, The training of MNNs on MNIST (left) and CIFAR-10 (right), with the accuracy (red line) and entropy (orange and green for correctly classified inputs and misclassified inputs respectively) on the test set. The shadows indicate the level of half standard deviations. As the training progresses, the entropy of correctly classified inputs and misclassified inputs diverges. **b**, The entropy of correctly classified and misclassified inputs in the last two layers of MNIST (left) and CIFAR-10 (right). The misclassified inputs result in relatively higher entropy in both layers. **c**, The entropy separability of correctly classified and misclassified inputs on MNIST (left) and CIFAR-10 (right) increases as the layer index increases. **d**, The relationship between the separability and test accuracy during training on MNIST (left) and CIFAR-10 (right) was analyzed using linear regression. The red dashed line represents the regression line, with coefficients of determination of 0.6803 for MNIST and 0.6068 for CIFAR-10.

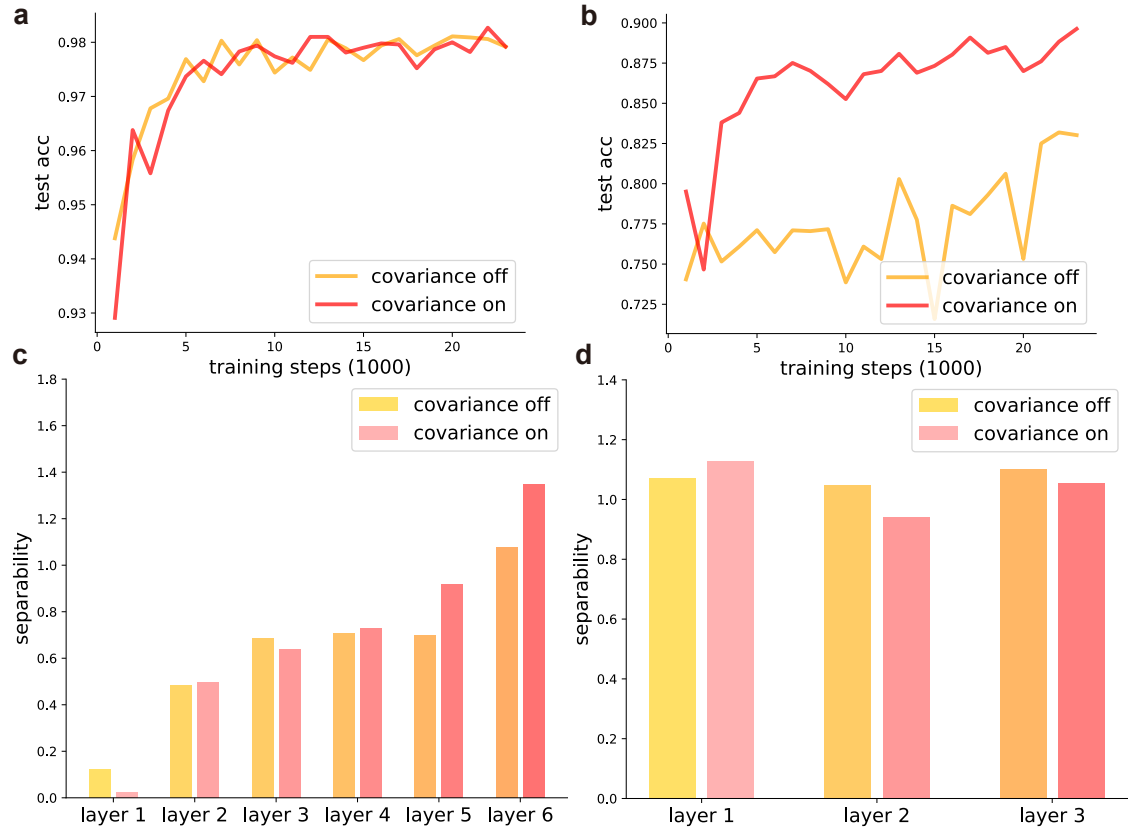


Figure S9: Comparison of MNNs with and without correlation. **a**, Test accuracy across training procedure for MNNs with and without correlation on MNIST classification. **b**, Test accuracy across training procedure for MNNs with and without correlation on CIFAR-10 classification. **c**, Entropy separability across layers procedure for MNNs with and without correlation on MNIST classification. **d**, Entropy separability across layers procedure for MNNs with and without correlation on CIFAR-10 classification.